Statistical Analysis of Moving-Base Gravimetry and Gravity Gradiometry

by

Christopher Jekeli

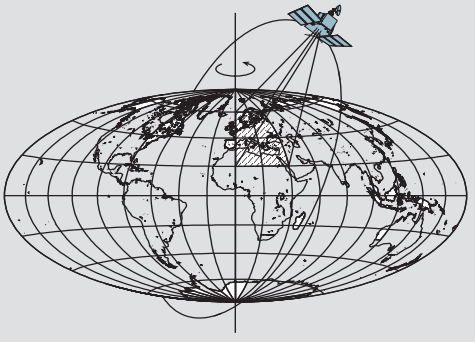

Report No. 466

Geodetic and GeoInformation Science
Department of Civil and Environmental Engineering and Geodetic Science
The Ohio State University
Columbus, Ohio 43210-1275

September 2003

Statistical Analysis of Moving-Base Gravimetry and Gravity Gradiometry

Christopher Jekeli
Laboratory for Space Geodesy and Remote Sensing Research
Geodetic Science
Ohio State University
2070 Neil Ave.
Columbus, OH 43210

tel: 614-292-7117
fax: 614-292-3780
e-mail: jekeli.1@osu.edu

TECHNICAL REPORT

prepared for

National Imagery and Mapping Agency
Attn: Dr. Randy Smith
12300 Sunrise Valley Drive MS P-53
Reston, VA 20191

Contract No. NMA202-98-1-1110
OSURF Project No. 736145

September 2003

Abstract

Moving-base gravimetry systems require multiple sensors to extract the gravitational signal – an accelerometer (or gravimeter), or a set of mutually orthogonal accelerometers that sense the action forces on the vehicle; a suite of gyroscopes (or a stabilized platform) that provides proper orientation for the accelerometers; and a geometric (kinematic) positioning system (e.g., GPS) from which the kinematic acceleration may be derived, and that also provides geospatial referencing of the signals. The error in the recovered gravitational signal depends on the individual sensor errors, but also on the coupling of the sensor errors to the actual acceleration environment of the system. The error analysis is fairly well known and documented in the literature and agrees largely with experimental and operational results. This report reviews the analysis in detail and extends it to moving-base gravity gradiometry. In the latter case the system comprises a set of gradiometers (or differential accelerometers), a suite of gyros for orientation (stabilization), and a geospatial referencing system (GPS). The errors in the recovered gravitational gradients depend on the sensor errors, but also on the coupling of these errors to the angular rate environment of the system. The analyses specifically target airborne systems used for gravity and gravity gradient mapping. While the orientation bias error is especially detrimental to airborne gravimetry, it is the random noise in the gyro angular rate that contributes most to airborne gradiometry, as it couples with the total angular rate. The analysis shows that a gradiometer with $1\ \mathrm{E}/\sqrt{\mathrm{Hz}}$ sensitivity will not be adversely compromised (at medium and high frequencies) if the required gyros have bias repeatability of $0.0015\ ^\circ/\mathrm{hr}$ and sensitivity of $0.01\ ^\circ/\mathrm{hr}/\sqrt{\mathrm{Hz}} \approx 0.00015\ ^\circ/\sqrt{\mathrm{hr}}$, and if the orientation bias is 0.06°. The latter numbers all reflect an order of magnitude lower than commensurate gradient error effects of $1\ \mathrm{E}/\sqrt{\mathrm{Hz}}$. This report also provides detailed models for the various error sources, as well as for the accelerations and angular rates of the aircraft and for the gravitational signal to wavelengths as short as 1 m.

I. Introduction

The purpose of this report is to understand the requirements and limitations of moving-base gravimetry systems, specifically those based on the accelerometer and the differential accelerometer (or gradiometer), to sense local and regional gravity anomalies. Much of this type of analysis was performed by many investigators in the past, and in that respect this report serves as a review. However, the gradiometry part is relatively new as it incorporates an analysis of the entire system, including the gyros that provide an orientation of the sensor platform and are needed to account for the angular velocities and accelerations. The analysis is presented starting from first principles, and particular attention is paid to developing appropriate models for the sensor errors and the gravitational field, the latter, especially, at very short spatial wavelengths, to which the gradiometer is particularly sensitive. Indeed, the gravitational field modeling is offered in the Appendices in complete detail in order to serve as reference for many different applications. In addition, models are developed for the acceleration and angular rate environment of a typical small airplane that might be used to carry such gravitational sensors.

The properties of the gravitational field are governed by Newton's *Law of Gravitation* which says that gravitational acceleration due to mass attraction attenuates with the inverse of the squared distance from the sources. The spatial derivatives of the gravitational acceleration, that is, its gradients, attenuate with the cube of the inverse distance. On the other hand, since the derivatives of a function describe its local behavior, the gravitational gradients, in some sense, compensate for the effect of attenuation; and, the gravitational gradiometer is viewed as particularly useful in detecting near-field (shallow) mass anomalies. Of course, the biggest advantage of the gradiometer is its insensitivity to common mode accelerations of the moving vehicle, meaning that no independent acceleration sensor is required as in the case of moving-base gravimetry. To have useful precision, however, the accelerometers in the pair that constitutes a gradiometer must be very well matched and aligned to avoid significant differential biases.

II. Mathematical Models for Measurements

This section develops the basic mathematical models for the gravitation vector and the gravity gradient tensor as determined from sensor system measurements. We consider several inertial sensors: the accelerometer as a primary sensor, the gravitational gradiometer (or, more precisely, the acceleration gradiometer) as a "derived" sensor (being a combination of accelerometers), and the gyroscope as an auxiliary sensor (providing orientation of the frame, as well as angular rates). A "position sensor" is also needed, and GPS is the now common utility for that function. According to Newton's *Second Law of Motion*, in an inertial (i.e., non-rotating) frame, the *i*-frame, we have

$$\ddot{\boldsymbol{x}}^i = \boldsymbol{g}^i + \boldsymbol{a}^i \quad , \tag{1}$$

where $\boldsymbol{g}^i$ is the gravitational acceleration, $\ddot{\boldsymbol{x}}^i$ is the total kinematic acceleration of the body, and $\boldsymbol{a}^i$ is the acceleration resulting from action forces ($\boldsymbol{a}^i$ is also called the *specific force*, and it is the acceleration actually sensed by an accelerometer). The superscript identifies the frame in which the vector is coordinatized; and, each dot on the vector, $\boldsymbol{x}$, denotes a differentiation with respect to time.

Let the *b*-frame (body-frame) be the coordinate frame in which the sensor operators. This can be an arbitrary frame that rotates (and accelerates) with respect to the *i*-frame. Let C_b^i denote the 3×3 matrix that rotates coordinates from the *b*-frame to the *i*-frame. This transformation matrix is orthogonal, and we have

$$\left(C_b^i\right)^{-1} = \left(C_b^i\right)^T = C_i^b \,, \quad \text{and} \quad C_i^b \, C_b^i = I \quad , \tag{2}$$

where *I* is the identity matrix. To rotate a vector from one frame to the other involves multiplying by this transformation matrix, e.g.:

$$\boldsymbol{a}^i = C_b^i \, \boldsymbol{a}^b \quad . \tag{3}$$

For later application, we note that, with the over-scripted dot denoting time-differentiation, as before,

$$\dot{C}_b^i = C_b^i \, \Omega_{ib}^b \,, \quad \text{where } \Omega_{ib}^b = \begin{pmatrix} 0 & -\omega_3 & \omega_2 \\ \omega_3 & 0 & -\omega_1 \\ -\omega_2 & \omega_1 & 0 \end{pmatrix} \quad , \tag{4}$$

and $\boldsymbol{\omega}_{ib}^{b} = \left(\omega_1 \; \omega_2 \; \omega_3 \right)^{\mathrm{T}}$ is the vector of angular rates of the *b*-frame axes with respect to the *i*-frame axes, coordinatized in the *b*-frame.

Substituting (3) into (1) yields:

$$\boldsymbol{g}^{i} = \ddot{\boldsymbol{x}}^{i} - C_{b}^{i} \boldsymbol{a}^{b} \quad . \tag{5}$$

Thus, in order to determine the gravitation vector from accelerometer data (in the *b*-frame), it is necessary to determine also $\ddot{\boldsymbol{x}}^{i}$, derived from the position, $\boldsymbol{x}^{i}$, and to know the orientation of the sensor platform with respect to inertial space. Once obtained in the *i*-frame, the gravitational vector can always be rotated into any other frame whose orientation with respect to the inertial frame is known, e.g.

$$\boldsymbol{g}^{n} = C_{i}^{n} \boldsymbol{g}^{i} \quad , \tag{6}$$

where the *n*-frame is the local north-east-down frame, and the elements of the rotation matrix, C_{i}^{n}, are functions of latitude, longitude, and Earth's rotation rate.

Modern gradiometers are based mostly on pairs of accelerometers whose outputs are differenced to yield the spatial gradient of acceleration, or the difference in acceleration per unit length (i.e., over the length of separation between the reference points of the accelerometers). We use the following, mathematically loose, notation to define the partial derivatives of components of a vector, say $\boldsymbol{a}$, with respect to components of another vector, say $\boldsymbol{x}$: $\partial \boldsymbol{a} / \partial \boldsymbol{x}$, given by:

$$\frac{\partial \boldsymbol{a}}{\partial \boldsymbol{x}} = \begin{pmatrix} \dfrac{\partial a_1}{\partial x_1} & \dfrac{\partial a_1}{\partial x_2} & \dfrac{\partial a_1}{\partial x_3} \\ \dfrac{\partial a_2}{\partial x_1} & \dfrac{\partial a_2}{\partial x_2} & \dfrac{\partial a_2}{\partial x_3} \\ \dfrac{\partial a_3}{\partial x_1} & \dfrac{\partial a_3}{\partial x_2} & \dfrac{\partial a_3}{\partial x_3} \end{pmatrix} \quad . \tag{7}$$

Before applying this type of gradient operator to an expression like equation (5), we must first express Newton's Law of Motion in the *b*-frame, the frame in which the spatial differentiation takes place (i.e., the frame of the sensor). Toward this end, we differentiate

$$\boldsymbol{x}^i = C_b^i \, \boldsymbol{x}^b \tag{8}$$

twice with respect to time and substitute equation (5):

$$\boldsymbol{g}^b = \ddot{\boldsymbol{x}}^b - \boldsymbol{a}^b + 2\, C_i^b \, \dot{C}_b^i \, \dot{\boldsymbol{x}}^b + C_i^b \, \ddot{C}_b^i \, \boldsymbol{x}^b \quad . \tag{9}$$

Now, differentiating with respect to $\boldsymbol{x}^b$, we find

$$\frac{\partial \boldsymbol{g}^b}{\partial \boldsymbol{x}^b} = -\frac{\partial \boldsymbol{a}^b}{\partial \boldsymbol{x}^b} + C_i^b \, \ddot{C}_b^i \quad , \tag{10}$$

since neither $\ddot{\boldsymbol{x}}^b$, $\dot{\boldsymbol{x}}^b$, nor C_b^i depend explicitly on $\boldsymbol{x}^b$. That is, the linear acceleration, $\ddot{\boldsymbol{x}}^b$, disappears, and the gravitational gradient can be obtained from the combination of gradiometer-sensed components, $\partial \boldsymbol{a}^b / \partial \boldsymbol{x}^b$, and the rotational acceleration, $C_i^b \, \ddot{C}_b^i$. It is important, therefore, that one is able to measure or otherwise determine the rotational dynamics of the platform on which the accelerometer pairs of a gradiometer are mounted. If the platform is *stabilized* in the *i*-frame, i.e., the *b*-frame is the *i*-frame, then, of course, $\dot{C}_b^i = \dot{C}_i^i = 0$, and the measurements yield directly the gravitational gradients.

Let Γ^b denote the matrix of gravitational gradients in the *b*-frame, that is, the tensor, $\partial \boldsymbol{g}^b / \partial \boldsymbol{x}^b$. Applying equation (4) twice in succession, we find that equation (10) is equivalent to

$$\Gamma^b = -\frac{\partial \boldsymbol{a}^b}{\partial \boldsymbol{x}^b} + \Omega_{ib}^b \Omega_{ib}^b + \dot{\Omega}_{ib}^b \quad . \tag{11}$$

If all components of the matrix, $\partial \boldsymbol{a}^b / \partial \boldsymbol{x}^b$, are measured, then we may take advantage of the facts that Γ^b is symmetric, while $\dot{\Omega}_{ib}^b$ is anti-symmetric, and thus eliminate the latter according to:

$$\begin{aligned} \Gamma^b &= \frac{1}{2}\left(\Gamma^b + \left(\Gamma^b\right)^{\mathrm{T}}\right) \\ &= -\frac{1}{2}\left(\frac{\partial \boldsymbol{a}^b}{\partial \boldsymbol{x}^b} + \left(\frac{\partial \boldsymbol{a}^b}{\partial \boldsymbol{x}^b}\right)^{\mathrm{T}}\right) + \Omega_{ib}^b \Omega_{ib}^b \\ &= -B^b + \Omega_{ib}^b \Omega_{ib}^b \, , \end{aligned} \tag{12}$$

where

$$B^b = \frac{1}{2}\left(\frac{\partial \boldsymbol{a}^b}{\partial \boldsymbol{x}^b} + \left(\frac{\partial \boldsymbol{a}^b}{\partial \boldsymbol{x}^b} \right)^{\mathrm{T}} \right) \quad . \tag{13}$$

We note that $\partial \boldsymbol{a}^b / \partial \boldsymbol{x}^b$ is not symmetric and so the relationship (12) yields all gravity gradients only if the gradiometer is a "full-tensor" gradiometer (all nine elements are measured independently). Of course, if one is interested merely in a subset of gradients, e.g., Γ^b_{13} and Γ^b_{23}, then avoiding the angular acceleration terms requires only measurements of $\partial a^b_1 / \partial x^b_3$, $\partial a^b_2 / \partial x^b_3$, $\partial a^b_3 / \partial x^b_1$, and $\partial a^b_3 / \partial x^b_2$. Or, if only Γ^b_{33} is desired, then the only gradient to be measured is $\partial a^b_3 / \partial x^b_3$. If elements of Γ are needed in another frame, such as the *n*-frame, then additional body-frame gradients must be measurements.

Indeed, to rotate the gradients into any other frame requires a further transformation. While vectors transform (rotate) according to (8), matrices, such as Γ, transform according to

$$\Gamma^i = C^i_b \, \Gamma^b \, C^b_i \quad . \tag{14}$$

Thus, we have

$$\Gamma^i = - C^i_b \left(B^b - \Omega^b_{ib} \Omega^b_{ib} \right) C^b_i \quad . \tag{15}$$

It may be noted that the term with the angular velocity (squared) within the parentheses is substantial compared to the gravitational gradients of the Earth. A body rotational rate of as little as $\omega = 10^{-3}$ rad/s = 3.5 arcmin/s implies an effect of $\omega^2 = 10^{-6}$ 1/s = 1000 Eötvös .

III. Error Equations

To develop error equations from the relationships between observables or sensor quantities and gravitational quantities, we use the δ-notation to denote small errors (i.e., errors are approximated by differential elements). (The notation, $\delta \boldsymbol{g}$, here used to represent the error in $\boldsymbol{g}$, is often used to denote the gravity disturbance vector. We denote the latter by $\Delta \boldsymbol{g}$, even though this notation is usually reserved to denote the gravity anomaly vector. But, in the planar approximation that we have adopted, the disturbance and the anomaly are almost the same.) Neglecting second-order terms, we have from equation (5):

$$\delta \boldsymbol{g}^i + \frac{\partial \boldsymbol{g}^i}{\partial \boldsymbol{x}^i}\, \delta \boldsymbol{x}^i = \delta \ddot{\boldsymbol{x}}^i - \delta C_b^i\, \boldsymbol{a}^b - C_b^i\, \delta \boldsymbol{a}^b \quad , \tag{16}$$

where the second term on the left side is due to the fact that the gravitational signal depends on position, and position is one of our observables that may be in error. This term is also known as a *registration error*. The error in the transformation matrix, δC_i^b, can be expressed (Jekeli, 2000, p.149) in terms of the orientation errors of the coordinate axes of the *b*-frame with respect to the *i*-frame, $\boldsymbol{\psi} = \begin{pmatrix} \psi_1 & \psi_2 & \psi_3 \end{pmatrix}^{\mathrm{T}}$:

$$\delta C_b^i = -\begin{pmatrix} 0 & -\psi_3 & \psi_2 \\ \psi_3 & 0 & -\psi_1 \\ -\psi_2 & \psi_1 & 0 \end{pmatrix} C_b^i = -\,\Psi\, C_b^i, \quad \delta C_i^b = \left(\delta C_b^i\right)^{\mathrm{T}} \quad . \tag{17}$$

The orientation errors are related to the errors in the angular rates, Ω_{ib}^b, according to

$$\frac{d}{dt}\Psi = -\,C_b^i\, \delta \Omega_{ib}^b\, C_i^b \quad . \tag{18}$$

With equation (17), equation (16) becomes:

$$\delta \boldsymbol{g}^i = \delta \ddot{\boldsymbol{x}}^i + \Psi\, C_b^i\, \boldsymbol{a}^b - C_b^i\, \delta \boldsymbol{a}^b - \Gamma^i\, \delta \boldsymbol{x}^i \quad . \tag{19}$$

Similarly, from equation (15) (using also equation (12)):

$$\delta \Gamma^i + \sum_j \frac{\partial \Gamma^i}{\partial x_j^i}\, \delta x_j^i = \delta C_b^i\, \Gamma^b\, C_i^b - C_b^i \left(\delta B^b - \delta \Omega_{ib}^b\, \Omega_{ib}^b - \Omega_{ib}^b\, \delta \Omega_{ib}^b \right) C_i^b + C_b^i\, \Gamma^b\, \delta C_i^b \quad . \tag{20}$$

Substituting equation (17) into equation (20) and making use of equation (14) yields

$$\delta\Gamma^i = \Gamma^i\,\Psi - \Psi\,\Gamma^i - C_b^i\left(\delta B^b - \delta\Omega_{ib}^b\,\Omega_{ib}^b - \Omega_{ib}^b\,\delta\Omega_{ib}^b\right)C_i^b - \sum_j \Xi_j^i\,\delta x_j^i \quad , \tag{21}$$

where Ξ_j^i is the gradient with respect to x_j^i of the gradient, Γ^i, and the last term, again, is a registration error.

For the simple error analyses to be conducted here, we may assume that the *b*-frame and *i*-frame coincide and are approximately equal to the local north-east-down frame (*n*-frame). This merely says that the platform of the instrument is aligned with the *n*-frame and the *n*-frame is approximately an inertial frame (for a short period of time, say, less than an hour). In that case the transformation matrix, C_b^i, is the identity matrix, and we can omit the sub- and superscripts that identify the different frames. Equations (19) and (21) become, in this special case,

$$\delta\boldsymbol{g} = \delta\ddot{\boldsymbol{x}} + \Psi\,\boldsymbol{a} - \delta\boldsymbol{a} - \Gamma\,\delta\boldsymbol{x} \quad , \tag{22}$$

$$\delta\Gamma = \Gamma\,\Psi - \Psi\,\Gamma - \delta B + \delta\Omega\,\Omega + \Omega\,\delta\Omega - \sum_j \Xi\,\delta x_j \quad . \tag{23}$$

Furthermore, from equation (18), we obtain, in this case,

$$\Psi = \Psi_0 - \int \delta\Omega\,dt \quad , \tag{24}$$

where Ψ_0 is a constant orientation error.

The error equations (22) and (23) are based on direct measurements of the acceleration components, their spatial derivatives, and angular rate components, which are typical, respectively, of accelerometers, differential accelerometers, and gyros. However, other types of sensors or sensor configurations may yield these basic quantities indirectly. For example, some gradiometers (for example, existing units used for airborne operations, Jekeli (1988), Talwani (2000)) yield measurements of combinations of in-line gradients (much like the Eötvös torsion balance, Nettleton (1976, pp.66-69). Also, Zorn (2002) recently proposed using a set of 12 accelerometers to sense both the linear and angular accelerations of a platform, thus eliminating the need for gyros. In these cases the error equations must be re-constructed to reflect the basic sensed quantities. Also, as considered above, one often desires not a particular component of the gradient tensor, but a combination of gradients, such as defined by the differential field curvature (Nettleton, 1976,

pp.70-71) (this may also be the case rarely for the gravity vector). The error equations for such quantities are simply combinations of errors already derived (based on a linearization), since these quantities are derived and not sensed directly.

Finally, it is noted that even though the gravitational gradients, according to equation (15) with $C_b^i = I$, are derived from a combination of elements of the measurement tensor, $\partial \boldsymbol{a}^b / \partial \boldsymbol{x}^b$, the variance-covariance matrix of the gradient errors due to errors in $\partial \boldsymbol{a}^b / \partial \boldsymbol{x}^b$ is a diagonal matrix if the measurement errors are uncorrelated (Appendix A), implying that also the computed gradients are uncorrelated (disregarding errors in the rotation rates).

IV. Power Spectral Density and Covariance Function

This section introduces the functions to be modeled for a statistical analysis of the errors in airborne gravimetry and gradiometry. Covariance functions and power spectral densities are needed not just for the sensor errors, but also for the signals being sensed, due to the fact that the error equations, though linear in the errors, nevertheless involve coupling terms containing the signal. The error analysis can be done most conveniently in the temporal frequency domain, since the sensor errors are usually characterized in terms of their behavior over different resolutions of time (e.g., long-period and short-period behavior). Analyzing the error with respect to frequencies yields its characterization in the *spectral domain*.

We denote by *f* the temporal frequency and by Φ the power in the signal per frequency, that is, the *power spectral density (psd)*. The psd is the spectral equivalent of the covariance; specifically, the spectral decomposition of the covariance function of a signal is its psd. Formally, the psd is the *Fourier transform* of the covariance function, $\phi(\tau)$, and vice versa:

$$\mathsf{F}(\phi) \equiv \Phi(f) = \int_{-\infty}^{\infty} \phi(\tau)\, e^{-i\,2\pi f\,\tau}\, d\tau\,, \quad \mathsf{F}^{-1}(\Phi) \equiv \phi(t) = \int_{-\infty}^{\infty} \Phi(f)\, e^{i\,2\pi f\,\tau}\, df \quad , \tag{25}$$

where the covariance is the statistical expectation of the product of a zero-mean signal, say *g*, at two different times, *t* and $t + \tau$:

$$\phi_g(\tau) = \mathsf{E}(g(t)\, g(t+\tau)) \quad . \tag{26}$$

Here, we assume a) that the signal is a stochastic process (one whose values at any time are associated with a probability function); b) that the statistics of this process are *stationary* (or, time-invariant; hence the covariance only depends on the time difference, τ); and c) that the statistics over time are equivalent to the statistics over probability space (this last property is known as *ergodicity*). Finally, as noted we assume that the mean (or statistical average) of the signal is zero; this is not essential, but simplifies the discussion and is the condition on which equation (26) is predicated. Since the psd is a *density* of signal power (the covariance) relative to frequency, its units are squared signal units per frequency units. In the temporal frequency domain, the units of frequency are usually cycles per second, or *Hertz [Hz]*.

There is, of course, a rich theory associated with the psd and covariance functions, which we can hardly touch upon here (for additional details, the reader may consult any textbook on stochastic processes, signal analysis, or probability theory (e.g., Papoulis, 1977; Priestley, 1981; see also Jekeli, 2001), but a number of special cases and facts must be illustrated. In analogy to the component wavelengths (inverse frequencies) of light, *white noise* is formally defined as the

error whose psd is constant over all frequencies (like white light that contains equal amounts of all colors, each color corresponding to a different frequency or wavelength). White noise is a perfectly uncorrelated stochastic process, since at any time it is completely random, independent of its value at any previous (or subsequent) time. An *bias* error, on the other hand, is a constant error and its psd is non-zero only at a single frequency, the zero-frequency. Such an error is perfectly correlated in time since it is known for all time once it is known for any instant in time.

Although the white noise and random bias processes will play significant roles in the subsequent analyses, other forms of partially correlated processes will be considered, such as red noise (also called *correlated noise*, where the error is dominated by components at the longer wavelengths or lower frequencies). In fact, similar to such errors, we assume that the signals themselves are correlated stochastic processes. That is, the (residual) accelerations and angular rates of an aircraft in straight and level flight are more or less random, as are the gravitational gradients (residual to some reference field). In all these cases, we assume the processes are of the type discussed above, that is, stationary and ergodic, and in most cases having zero mean. Furthermore, we assume that the errors are not correlated between the different sensors and that, in general, sensor errors are not correlated with the quantities being sensed.

The power spectral density of the gravitational field, assumed to be a correlated process on the sphere, is defined over the spectral domain of two-dimensional spatial frequencies, or harmonic orders and degrees (or, wavenumbers). Specifically, the spectral decomposition of the gravitational potential, *V*, on any sphere of radius, *r*, is an infinite series of spherical harmonics:

$$V(r,\theta,\lambda) = \sum_{n=0}^{\infty} \sum_{m=-n}^{n} \left(\frac{R}{r}\right)^{n+1} \nu_{n,m}\, \bar{Y}_{n,m}(\theta,\lambda) \quad , \tag{27}$$

where θ,λ are spherical co-latitude and longitude, $\bar{Y}_{n,m}$ is a spherical harmonic function of degree *n* and order *m*, and the set of coefficients, $\{\nu_{n,m}\}$, constitutes the spectrum of *V*. The radius, *R*, is some mean Earth radius, and we may choose $r = R$ when considering the spherical spectrum of *V* on the Earth's surface. $\bar{Y}_{n,m}$ is the product of Legendre functions of the first kind and sines and cosines (see any book on mathematical physics or physical geodesy, such as Heiskanen and Moritz, 1967).

For our more local analyses, the spherical frequencies may be approximated by spatial frequencies in the (horizontal) plane:

$$\frac{\sqrt{n(n+1)}}{2\pi R} = \mu\,, \quad \mu = \sqrt{\mu_1^2 + \mu_2^2} \quad , \tag{28}$$

where μ is the "amplitude" of the horizontal (Cartesian) spatial frequencies, μ_1 and μ_2.

The spherical psd of the function, such as *V*, is given, usually, as the cumulative density per

degree, or the *degree variance*:

$$\sigma_V^2(n) = \sum_{m=-n}^{m} v_{nm}^2 \quad . \tag{29}$$

It can be shown (Jekeli, 2001) that the relationship between the degree variance and the isotropic psd, $\Phi_V(\mu)$, of signals on the plane is given by

$$\sigma_V^2(n) \approx \frac{n}{2\pi R^2}\, \Phi_V(\mu) \quad . \tag{30}$$

Note that, even, though $\Phi_V(\mu)$ is the psd depending only on the amplitude frequency, μ, it is nevertheless the psd for a signal in two dimensions (on the plane), and as such its units are the square units of *V* per the *square* of the frequency units.

Modeling the power spectral density of the gravitational signal usually involves the analysis of different types of data. For the medium to longer wavelengths, satellite tracking data and mean terrestrial gravity anomalies estimated on a uniform grid (e.g., $0.5^\circ \times 0.5^\circ$) serve to generate spectral decompositions of *V*, as given by equation (27). One such global representation is EGM96 (Lemoine et al., 1998), where the maximum degree is $n_{\max} = 360$ (corresponding to a spatial resolution of about 25 km). To model the field at higher resolution we must rely on more dense gravimetric data. Alternatively, over land areas, we may utilize detailed grids of terrain elevation under the assumption that the very-high frequency anomalies of the gravity field are generated principally by the visible terrain variations, and possibly by corresponding isostatic compensations, e.g., according to the Airy model.

To simplify the relationship between the gravitational field and the topographic heights, we approximate the topography by its Helmert condensation onto the geoid. The topographic masses thus are "condensed" onto the geoid in the form of a two-dimensional mass layer with density given at any point by

$$\kappa = \rho h \quad , \tag{31}$$

where ρ is the crustal density (assumed constant, in our model) and *h* is the terrain elevation at this point. The potential, *V*, at a point, *P*, due to such a layer is given by

$$V(P) = G\rho R^2 \int\!\!\int_{\sigma} \frac{h}{\ell}\, d\sigma \quad , \tag{32}$$

where G is Newton's gravitational constant, σ represents the unit sphere, h is a function of spherical coordinates, being approximations of some curvilinear coordinates on the geoid, and ℓ is the distance between P and the integration point. The potential and its derivatives are continuous, as long as P is located above the surface.

Equation (32) is a convolution of h with the inverse distance, ℓ^{-1}. Further approximating the coordinates as planar coordinates, where now

$$\ell = \sqrt{\left(x_1 - x_1'\right)^2 + \left(x_2 - x_2'\right)^2 + x_3^2} \quad , \tag{33}$$

and $\left(x_1', x_2'\right)$ are coordinates of points on the geoid, one may apply the convolution theorem to show that the Fourier transform of the potential at the level of $x_3 \geq 0$ is given by (Jekeli, 2001, pp.1-32)

$$\mathsf{F}(V) = \frac{k\rho}{\mu}\, \mathsf{F}(h)\, \mathrm{e}^{-2\pi\mu x_3} \quad , \tag{34}$$

where μ is given by equation (28). Therefore, the (cross-) psd of the potential at two levels, x_3 and x_3', is given by

$$\Phi_V\left(\mu; x_3, x_3'\right) = \left(\frac{k\rho}{\mu}\right)^2 \Phi_h(\mu)\, \mathrm{e}^{-2\pi\mu\left(x_3 + x_3'\right)} \quad . \tag{35}$$

And, consequently, the psd of the vertical derivative of V (the gravitational acceleration of a layer) is given by

$$\Phi_{\delta g}\left(\mu; x_3, x_3'\right) = \left(2\pi k\rho\right)^2 \Phi_h(\mu)\, \mathrm{e}^{-2\pi\mu\left(x_3 + x_3'\right)} \quad . \tag{36}$$

If one includes a model for isostatic compensation of the topographic layer, say, according to Airy's hypothesis, then another layer can be formed on the underside of the zone of compensation, extending a depth, D, below the geoid. This layer has density $\kappa' = -\left(\rho_m - \rho\right) h'$, representing a condensation of material *deficient* in density with respect to the mantle density, ρ_m, and extending a depth, h', below the level $-D$ (see Figure 1). The Airy model is based on the buoyancy of the topographic masses floating in the mantle; thus we have

$$\rho\, h = \left(\rho_m - \rho\right) h' \quad . \tag{37}$$

Including this anomalous layer, with density $\kappa' = -\rho\, h$, the Fourier transform of the total potential

due to both topography and its isostatic compensation, approximated as surface layers, is given by

$$\mathsf{F}(V) = \frac{k\rho}{\mu}\,\mathsf{F}(h)\left(e^{-2\pi\mu x_3} - e^{-2\pi\mu(D+x_3)}\right) \quad . \tag{38}$$

And, the (cross-) psd at two arbitrary levels, x_3 and x_3', is given by

$$\Phi_V(\mu; x_3, x_3') = \left(\frac{k\rho}{\mu}\right)^2 \Phi_h(\mu)\, e^{-2\pi\mu(x_3 + x_3')}\left(1 - e^{-2\pi\mu D}\right)^2 \quad . \tag{39}$$

Finally, the psd of the corresponding vertical gravitational acceleration is given by

$$\Phi_{\delta g}(\mu; x_3, x_3') = (2\pi k\rho)^2\, \Phi_h(\mu)\, e^{-2\pi\mu(x_3 + x_3')}\left(1 - e^{-2\pi\mu D}\right)^2 \quad . \tag{40}$$

It is noted that equations (36) and (40) basically state that the gravity disturbance (or anomaly) is linearly related to elevation, which is a common (though not necessarily legitimate) assumption made in short-wavelength analyses of the gravity field. Also, if the isostatic compensation should be omitted, equation (40) can be used as well simply by setting $D \to \infty$. In fact, for a typical compensation depth, D = 30 km , the isostatic compensation factor is

$$e^{-2\pi\mu D} \le 0.002\,, \quad \text{for } \mu \ge 3.3\times10^{-5}\ \text{cy/m}\ ; \tag{41}$$

which can be neglected if the gravity is modeled from topography only at resolutions (half-wavelengths) more detailed than $D/2$ = 15 km .

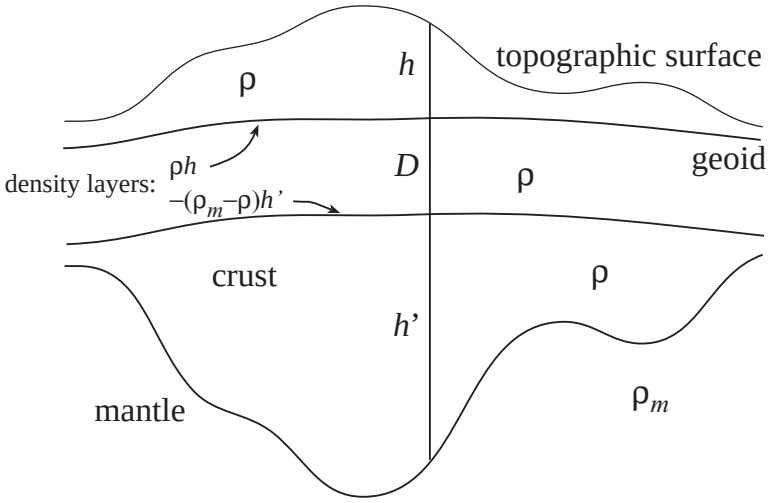

Figure 1: Airy's isostatic compensation model and Helmert's condensation layers

V. Covariance and PSD Models

Having identified the types of covariance functions and psd's to be modeled, we now develop specific models to be used for the individual sensors and the accelerations and angular rates of a typical aircraft, and for the gravitational signal. Finally, a total, combined model is developed for the error in the determined components of the gravitational vector and the gradient tensor.

The Fourier relationships (25) between the covariance and psd are problematic in the two cases of white noise and bias, since, for example, the integral of a function that is non-zero at only a single value of its domain is zero in the usual Riemann / Lebesque sense of an integral. To avoid such degeneracy, one introduces a *generalized function*, the *Dirac* function (also known as the *delta* function, or the *impulse* function, not to be confused with the differential operator, δ, used above), defined by the following:

$$\delta(t) = 0 , \quad \text{for } t \neq 0 ;$$
$$\int_{-\infty}^{\infty} \delta(t - t_0)\, g(t)\, dt = \int_{-\infty}^{\infty} \delta(t_0 - t)\, g(t)\, dt = g(t_0) . \tag{42}$$

Thus, if we let the covariance function of white noise be a Dirac function, scaled by a constant, $w > 0$; then by equations (25) and (42), with $t_0 = 0$ and $t \equiv \tau$, the psd is that constant:

$$\phi(\tau) = w\, \delta(\tau) \quad \Rightarrow \quad \Phi(f) = \int_{-\infty}^{\infty} w\, \delta(\tau)\, e^{-i\, 2\pi f\, \tau}\, d\tau = w \ . \tag{43}$$

Similarly, if the psd is a Dirac function, scaled by σ^2, then the covariance function is that constant, for all τ, as desired for a random bias:

$$\Phi(f) = \sigma^2\, \delta(f) \quad \Rightarrow \quad \phi(\tau) = \int_{-\infty}^{\infty} \sigma^2\, \delta(f)\, e^{i\, 2\pi f\, \tau}\, df = \sigma^2 \ . \tag{44}$$

We note that the units of the Dirac function, as inferred from (42), are the *inverse* of the units of the argument of $\delta(\cdot)$.

On the other hand, we quickly encounter difficulties when implementing these idealizations of

white noise and random bias in modeling the psd's of derived quantities, such as the psd of kinematic acceleration error, given the psd of position error. Mathematically, the psd of the acceleration error is obtained with multiple differentiations of the psd of position error, which becomes difficult when dealing with the Dirac function. To enable straightforward manipulation of our psd's, we approximate the ideal white noise and random bias with processes that behave accordingly only over a finite bandwidth of frequencies (in fact, one can argue that this is more realistic, anyway), thus yielding analytic functions for the psd's.

Several options exist for analytic expressions (i.e., regular, reasonably well-behaved functions) of the psd and covariance function that are Fourier transforms of each other, according to equation (25), and that can be tailored to approximate band-limited white noise and random bias. One such transform pair is given by

$$\phi(\tau) = \sigma^2 \frac{\sin(2\pi f_c \tau)}{2\pi f_c \tau} \ ; \tag{45}$$

$$\Phi(f) = \begin{cases} \dfrac{\sigma^2}{2f_c}, & |f| \le f_c, \\ 0, & |f| > f_c; \end{cases} \ . \tag{46}$$

where the positive parameter, f_c, controls the bandwidth of the signal. However, in this case, the attenuation of the psd and covariance is not controllable; and, therefore, this transform pair will not be used.

Instead, consider the following transform pair, here called type *A*:

$$\phi_A(\tau) = \frac{2 f_c \sqrt{\pi}\, w}{\Gamma\left(m + \frac{1}{2}\right)} \left(\pi f_c |\tau|\right)^m K_m(2\pi f_c |\tau|) \ , \tag{47}$$

$$\Phi_A(f) = \frac{w}{\left(1 + \left(\dfrac{f}{f_c}\right)^2\right)^{m+\frac{1}{2}}} \ , \tag{48}$$

where $\Gamma(m)$ is the Euler-Gamma function, with $\Gamma(m) = (m-1)!$, if m is a positive integer (confusion in notation with the gravitational gradients is not anticipated), and K_m is the modified Bessel function of the second kind and of order *m*. The order, *m*, of the Bessel function may, in this case, be a complex number with $\mathrm{Re}(m) > -\frac{1}{2}$; we will use only real *m*. That equations (47) and (48) satisfy equation (25) can be proved using formulas 9.6.9 and 9.6.25 in (Abramowitz and Stegun, 1972).

This model is particularly useful when we are given the psd value, *w*, of the process near zero frequency (e.g., white noise) and the cut-off frequency, f_c, that determines the bandwidth of the process. The parameter, *m*, determines the degree of attenuation of the psd. The variance of the process according to this model is given by

$$\phi_A(0) = \sigma^2 = \frac{w\, f_c \sqrt{\pi}\ \Gamma(m)}{\Gamma\left(m + \frac{1}{2}\right)} \tag{49}$$

We also note that

$$\Phi_A(f) > 0\ ,\ \forall f\ , \tag{50}$$

which means that the covariance function is positive definite as required.

Although one could use the Type *A* model to represent white noise as well as random bias processes with appropriate selection of the parameters, we consider also the inverse of this model, here called Type *B*:

$$\phi_B(\tau) = \frac{\sigma^2}{\left(1 + \left(\frac{\tau}{\tau_c}\right)^2\right)^{m+\frac{1}{2}}}\ , \tag{51}$$

$$\Phi_B(f) = \frac{2\,\sigma^2\,\tau_c\sqrt{\pi}}{\Gamma\left(m + \frac{1}{2}\right)} \left(\pi\,\tau_c\,|f|\right)^m K_m\left(2\pi\,\tau_c\,|f|\right)\ . \tag{52}$$

This model is useful if the variance, σ^2, of the process is given. Here, the positive parameter, τ_c, defines the correlation length of the process. Again, the parameter, *m*, is restricted as for Type *A*, and the psd is always positive. The psd of Type *A* is modeled after the Butterworth filter and the covariance of Type *B* is a generalized inverse time function.

One must exercise some care when choosing a particular type of model. For example, by the propagation of covariances, with $\tau = |t_2 - t_1|$, the (cross-) covariance between time-derivatives of two processes, *g* and *h*, is given by

$$\phi_{\dot{g},\dot{h}}(\tau) = \frac{\partial}{\partial t_1}\frac{\partial}{\partial t_2}\phi_{g,h}(\tau) = -\frac{d^2}{d\tau^2}\phi_{g,h}(\tau)\ . \tag{53}$$

From (Abramowitz and Stegun, 1972, 9.6.28), we find that

$$\frac{d^k}{d\tau^k}\left((2\pi f_c\tau)^m K_m(2\pi f_c\tau)\right) = (-1)^k (2\pi f_c)^k (2\pi f_c\tau)^m K_{m-k}(2\pi f_c\tau) \quad , \tag{54}$$

which yields the nonsensical result that the variances are zero for the time-derivatives of a process whose covariance is modeled according to a Type *A* function, equation (47). Thus, when modeling the covariance or psd of the derivative of a process, the Type *B* model should be used. The psd of the k^{th} derivative of a process, *g*, is given by

$$\Phi_{g^{(k)}}(f) = (2\pi f)^{2k}\, \Phi_g(f) \quad , \tag{55}$$

and the covariance can be determined by applying equation (53) (repeatedly, if needed) to equation (51).

The covariance of the *integral* of a process is also relatively easy to formulate analytically for Type *B* models. However, if the covariance function of the original process does not average to zero over all τ (i.e., the psd has non-zero value at zero frequency), the integral of the process is non-stationary and the corresponding psd is not defined. Nevertheless, if we exclude a small neighborhood of frequencies at $f = 0$, then we may consider the psd of the integral of a process according to

$$\Phi_{\int g}(f) = \frac{1}{(2\pi f)^2}\, \Phi_g(f) \quad . \tag{56}$$

Usually we are interested only in a particular band of frequencies that excludes the origin and where the psd behaves according to (56). In this case we may fit a model of Type *A* to $\Phi_{\int g}$ over the bandwidth of interest. For example, if *g* is white noise with psd, $\Phi_g(f) = w_g$, for $f < f_g$, then

$$\Phi_{\int g}(f) = \frac{w_g}{(2\pi f)^2} \quad . \tag{57}$$

Fitting a Type *A* model (equation (48)) to this for $f > f_c$, we find that for $f_c < f < f_g$ these models approximately agree if

$$m = \frac{1}{2}, \quad w = \frac{w_g}{(2\pi f_c)^2} \quad . \tag{58}$$

Similarly, if g is a random bias with variance, σ_g^2 and correlation length, τ_g, then for frequencies, $f > 1/\tau_g$, we have, approximately, according to equations (49) and (48):

$$\Phi_g(f) = \frac{\sigma_g^2 \, \tau_g \, \Gamma\left(m_g + \frac{1}{2}\right)}{\sqrt{\pi}\, \Gamma(m_g)} \, \frac{1}{(f\,\tau_g)^{m_g + 1/2}} \quad , \tag{59}$$

for some m_g. Again, approximating the corresponding psd of the integral by a model of Type *A*, we set

$$m = m_g + 1 \, , \quad f_c = \frac{1}{\tau_g \, \alpha} \, , \quad w = \frac{\sigma_g^2 \, \tau_g \, \Gamma\left(m_g + \frac{1}{2}\right)}{\sqrt{\pi}\, \Gamma(m_g)} \, \frac{\alpha^{2m_g + 1}}{(2\pi f_c)^2} \quad , \tag{60}$$

where α is a fitting parameter (e.g., close to unity) that improves the fit.

For red noise processes, we again use the model of Type *A*, with suitable choices for the parameters. Indeed, suppose the psd over a certain band of frequencies, $f >> f_c$, should be modeled according to

$$\Phi(f) = \alpha f^{-\nu} \tag{61}$$

where α and ν are positive constants with $\nu > 1$. Over this band, we find from equation (48) that the Type *A* model may approximated as

$$\begin{aligned} \Phi(f) &= w \left(\frac{f_c}{f}\right)^{2m+1} \left(1 - \left(m + \frac{1}{2}\right)\left(\frac{f_c}{f}\right)^2 + \ldots\right) \\ &\approx w \left(\frac{f_c}{f}\right)^{2m+1} \, . \end{aligned} \tag{62}$$

Given α, ν, and f_c, one simply sets

$$m = \frac{1}{2}(\nu - 1) \, , \quad w = \alpha f_c^{-2m-1} \, . \tag{63}$$

For the gravitational processes, we define a covariance model analogous to Type *B*. This is a standard model for the covariance function of the *disturbing potential*, *T*, called the *reciprocal distance model* (Moritz, 1980). It is equation (51) specialized with $m = 0$ and generalized by

including the Newtonian field condition; we call it a model of Type *C*:

$$\phi_T\left(\Delta x_1,\Delta x_2; x_3,x_3'\right) = \sum_{j=1}^{J} \frac{\sigma_j^2}{\sqrt{\left(1+\alpha_j\left(x_3+x_3'\right)\right)^2+\alpha_j^2 s^2}} \quad , \tag{64}$$

where

$$\Delta x_1 = x_1 - x_1' \,, \quad \Delta x_2 = x_2 - x_2' \,, \quad s = \sqrt{\Delta x_1^2 + \Delta x_2^2} \,, \tag{65}$$

and where J, σ_j, and α_j are parameters whose values are selected to fit an empirical determination of the covariance or the psd. The psd model corresponding to equation (64) is given by

$$\Phi_T\left(\mu_1,\mu_2; x_3,x_3'\right) = \sum_{j=1}^{J} \frac{\sigma_j^2 \, \mathrm{e}^{-2\pi\mu\alpha_j^{-1}}}{\alpha_j \, \mu} \mathrm{e}^{-2\pi\mu\left(x_3+x_3'\right)} \,, \tag{66}$$

where μ is given by equation (28). Covariance and psd models for the first and second derivatives of the disturbing potential are easily derived and listed in Appendix B.

To utilize the gravitational signal spectra along a track requires that the two-dimensional spatial psd be collapsed to a single dimension, where it is assumed that the track can be identified with one of the horizontal coordinate axes. We define the following hybrid psd/covariance function for the disturbing potential:

$$\begin{aligned} S_T\left(\mu_1; \Delta x_2; x_3,x_3'\right) &= \int_{-\infty}^{\infty} \Phi_T\left(\mu_1, \mu_2; x_3,x_3'\right) \mathrm{e}^{i\,2\pi\mu_2\Delta x_2} d\mu_2 \\ &= \int_{-\infty}^{\infty} \phi_T\left(\Delta x_1, \Delta x_2; x_3,x_3'\right) \mathrm{e}^{-i\,2\pi\mu_1\Delta x_1} \, d\Delta x_1 \,, \end{aligned} \tag{67}$$

and this yields the *along-track psd* by setting $\Delta x_2 = 0$. Here, without loss in generality, we assume that x_1 represents the along-track direction. In the case of the reciprocal-distance model (Type *C*), this hybrid psd/covariance function has closed analytic expressions for the disturbing potential and all its derivatives; these are listed in Appendix C.

In order to proceed with the analysis, we need some additional results. It is easy to see that the covariance of the sum or difference of two uncorrelated processes is the sum of the covariances of the processes:

$$\phi_{A \pm B}(f) = \phi_A(f) + \phi_B(f) \quad . \tag{68}$$

For the *product* of a signal, g (like $\boldsymbol{a}$, Γ, or ω), and an error, ε (like δx, etc.), we make use of the ergodic property to derive the covariance sequentially, as follows. Assume, first, that the covariance of the product, $g\varepsilon$, is obtained in the probability space (again, both are zero-mean processes):

$$\phi_{g\varepsilon}(t,\tau) = \mathsf{E}\Big(g(t)\varepsilon(t)\, g(t+\tau)\varepsilon(t+\tau)\Big) = g(t)\, g(t+\tau)\, \phi_\varepsilon(\tau) \quad , \tag{69}$$

where $g(t)$ and $g(t+\tau)$ are treated like constants (from a completely different probability space) that pre-multiply the errors. Next, average this over all possible values of t, in effect computing the (time-averaged) covariance of g:

$$\begin{aligned} \phi_{g\varepsilon}(\tau) &= \lim_{T\to\infty} \frac{1}{T} \int_{-T/2}^{T/2} g(t)\, g(t+\tau)\, \phi_\varepsilon(\tau)\, dt \\ &= \phi_g(\tau)\, \phi_\varepsilon(\tau) \,. \end{aligned} \tag{70}$$

According to well known theorems in Fourier analysis, the Fourier transform of the product, $\phi_g\, \phi_\varepsilon$, is the convolution of the Fourier transforms of ϕ_g and ϕ_ε. This leads to the result that the psd of $g\varepsilon$ is the *convolution* of the psd's of g and of ε:

$$\Phi_{g\varepsilon}(f) = \int_{-\infty}^{\infty} \Phi_g(f')\, \Phi_\varepsilon(f-f')\, df' \quad . \tag{71}$$

Unfortunately, however, our psd models of Type *A*, equation (48), Type *B*, equation (52), and Type *C*, equation (66), do not yield simple analytic expressions when substituted into equation (71).

Therefore, where necessary, the following procedure is adopted. We first design the covariances of the signals and errors based on appropriate models and spectral characteristics. These are then combined according to equations (68) and (70), and the psd of the resulting

expression is determined *numerically* according to equation (25).

The operative models for the gravitational estimation errors are equations (22) and (23). In equation (22) we consider separately the vertical and horizontal components of the gravitational vector (and the two horizontal components are essentially equivalent):

$$\Phi_{\delta g_1} = \Phi_{\delta\ddot{x}_1} + \Phi_{\psi_3 a_2} + \Phi_{\psi_2 a_3} + \Phi_{\delta a_1} + \Phi_{\Gamma_{11}\delta x_1} + \Phi_{\Gamma_{12}\delta x_2} + \Phi_{\Gamma_{13}\delta x_3} \quad , \tag{72}$$

$$\Phi_{\delta g_3} = \Phi_{\delta\ddot{x}_3} + \Phi_{\psi_2 a_1} + \Phi_{\psi_1 a_2} + \Phi_{\delta a_3} + \Phi_{\Gamma_{31}\delta x_1} + \Phi_{\Gamma_{32}\delta x_2} + \Phi_{\Gamma_{33}\delta x_3} \quad . \tag{73}$$

For the gravitational gradients, let the indices j, k, ℓ denote a cyclical permutation of 1, 2, 3 (i.e., (1,2,3), (2,3,1), or (3,1,2)). Then the psd's of the errors in the diagonal gradients are given by:

$$\begin{aligned} \Phi_{\delta\Gamma_{j,j}} = {} & 4\Phi_{\Gamma_{j,k}\psi_\ell} + 4\Phi_{\Gamma_{\ell,j}\psi_k} + \Phi_{\delta(\partial a_j/\partial x_j)} \\ & 4\Phi_{\delta\omega_k\omega_k} + 4\Phi_{\omega_\ell\delta\omega_\ell} + \Phi_{\partial\Gamma_{j,j}/\partial x_1\delta x_1} + \Phi_{\partial\Gamma_{j,j}/\partial x_2\delta x_2} + \Phi_{\partial\Gamma_{j,j}/\partial x_3\delta x_3} \end{aligned} \tag{74}$$

And, for the off-diagonal gradient errors:

$$\begin{aligned} \Phi_{\delta\Gamma_{j,k}} = {} & \Phi_{\Gamma_{j,j}\psi_\ell} + \Phi_{\Gamma_{k,k}\psi_\ell} + \Phi_{\Gamma_{j,\ell}\psi_j} + \Phi_{\Gamma_{k,\ell}\psi_k} + \frac{1}{4}\Phi_{\delta(\partial a_j/\partial x_k)} + \frac{1}{4}\Phi_{\delta(\partial a_k/\partial x_j)} \\ & \Phi_{\delta\omega_j\omega_k} + \Phi_{\omega_j\delta\omega_k} + \Phi_{\partial\Gamma_{j,k}/\partial x_1\delta x_1} + \Phi_{\partial\Gamma_{j,k}/\partial x_2\delta x_2} + \Phi_{\partial\Gamma_{j,k}/\partial x_3\delta x_3} \end{aligned} \tag{75}$$

VI. Sensor Error Covariance Models

This section defines the models and associated parameters for the sensor errors $\delta \boldsymbol{a}$, $\delta(\partial \boldsymbol{a}/\partial \boldsymbol{x})$, $\delta \boldsymbol{x}$, and $\delta \boldsymbol{\omega}$, respectively, corresponding to the accelerometer, the gradiometer, GPS, and the gyroscope. Each sensor may be subject to a variety of types of errors, including white noise, red noise, random biases, scale factor errors, and errors correlated with ambient atmospheric, electromagnetic, and dynamic conditions. Some of these systematic errors are specific to a particular brand of instrument and are determined to some extent during the self-calibration phase of their operation. Others are significantly less important than the most basic of errors, the random bias and white noise, that we will consider here. Of course, there may be still other errors that elude the discussion here and yet are decidedly important. These contribute to the approximations and simplifications inherent in our analyses.

Geodetically precise GPS positions are determined from the phase of the carrier wave transmitted by the satellites and collected by the terrestrial receiver. The noise of the phase measurement is essentially white (uncorrelated), which has been confirmed by several investigators (e.g., Jekeli, 1992; Bona, 2000; Bona and Tiberius, 2000), and has a standard deviation as small as a few tenth of a millimeter. However, the positions derived for a moving platform, such as an aircraft, typically have errors with standard deviations of the order of a few centimeters (Grejner-Brzezinska et al., 1998), and we adopt a conservative standard deviation, $\sigma_{\delta x} = 10$ cm. A Type *B* model is used to represent the psd of the position error, assumed to be white noise for frequencies, $f < 1/\tau_{\delta x}$. Then the psd of the derived acceleration is given by

$$\Phi_{\delta \ddot{x}}(\tau) = (2\pi f)^4 \frac{2\,\sigma_{\delta x}^2\,\tau_{\delta x}\sqrt{\pi}}{\Gamma\left(m_{\delta x}+\frac{1}{2}\right)} \left(\pi\,\tau_{\delta x}\,|f|\right)^{m_{\delta x}} K_{m_{\delta x}}\left(2\pi\,\tau_{\delta x}\,|f|\right) \quad . \tag{76}$$

Values for the parameters, including the attenuation factor, $m_{\delta x}$, are given in Table 1.

For the inertial accelerometer, most manufacturers provide an estimate of the statistical nature of a random bias and white noise for the error, usually in the form of variances and psd's. The unknown bias, of course, primarily affects the zero-frequency in the gravitational signal, that is, its constant part, if the trajectory is straight and level. In general, its effect is modulated by C_b^i, as seen in equation (16), but in our simplified analysis ($C_b^i \approx I$), it is omitted. A Type *A* or *B* model can be used to represent the white noise, depending, respectively, on whether the psd amplitude or the standard deviation of the noise is provided. Assuming the standard deviation, $\sigma_{\delta a}$, is given, we model the white-nose psd as Type *B*:

$$\Phi_{\delta a}(f) = \frac{2\,\sigma_{\delta a}^2\,\tau_{\delta a}\sqrt{\pi}}{\Gamma\left(m_{\delta a}+\frac{1}{2}\right)}\left(\pi\,\tau_{\delta a}\,|f|\right)^{m_{\delta a}} K_{m_{\delta a}}\left(2\pi\,\tau_{\delta a}\,|f|\right)\,, \tag{77}$$

with suitably chosen time constant, $\tau_{\delta a}$, and attenuation parameter, $m_{\delta a}$ (see Table 1).

The gyros, which provide the orientation of the accelerometers and gradiometers, are subject at least to a random bias, $\delta\omega_0$, and white noise, $\delta\omega_w$, in the sensed angular rate, so that we assume

$$\delta\omega = \delta\omega_0 + \delta\omega_w\ , \tag{78}$$

and, according to equation (24),

$$\psi = \psi_0 - \int \left(\delta\omega_0 + \delta\omega_w\right) dt\ . \tag{79}$$

Again, manufacturers generally provide some statistical information for these basic error types. Orientation and angular rate errors couple with the signal according to equation (22) for the gravity components and equation (23) for the gradients. Adopting a Type *B* model for the angular rate bias and a Type *A* model for the white noise in the angular rate, we have

$$\phi_{\delta\omega}(\tau) = \frac{\sigma_{\delta\omega_0}^2}{\left(1+\left(\frac{\tau}{\tau_{\delta\omega_0}}\right)^2\right)^{m_{\delta\omega_0}+\frac{1}{2}}} + \frac{2\,f_{\delta\omega_w}\sqrt{\pi}\,w_{\delta\omega_w}}{\Gamma\left(m_{\delta\omega_w}+\frac{1}{2}\right)}\left(\pi\,f_{\delta\omega_w}\,|\,\tau|\right)^{m_{\delta\omega_w}} K_{m_{\delta\omega_w}}\left(2\pi\,f_{\delta\omega_w}\,|\,\tau|\right)\ , \tag{80}$$

where parameter values are given in Table 1.

Corresponding orientation error *covariances* are based on equation (79) and on psd approximations of equations (57) and (59) by Type *A* models:

$$\begin{aligned}\phi_{\psi}(\tau) = \sigma_{\psi_0}^2 &+ \frac{2\,f_{\psi/\delta\omega_w}\sqrt{\pi}\,w_{\psi/\delta\omega_w}}{\Gamma\left(m_{\psi/\delta\omega_w}+\frac{1}{2}\right)}\left(\pi\,f_{\psi/\delta\omega_w}\,|\,\tau|\right)^{m_{\psi/\delta\omega_w}} K_{m_{\psi/\delta\omega_w}}\left(2\pi\,f_{\psi/\delta\omega_w}\,|\,\tau|\right)\\ &+ \frac{2\,f_{\psi/\delta\omega_0}\sqrt{\pi}\,w_{\psi/\delta\omega_0}}{\Gamma\left(m_{\psi/\delta\omega_0}+\frac{1}{2}\right)}\left(\pi\,f_{\psi/\delta\omega_0}\,|\,\tau|\right)^{m_{\psi/\delta\omega_0}} K_{m_{\psi/\delta\omega_0}}\left(2\pi\,f_{\psi/\delta\omega_0}\,|\,\tau|\right),\end{aligned} \tag{81}$$

where the parameters, $f_{\psi/\delta\omega_w}$, $w_{\psi/\delta\omega_w}$, and $m_{\psi/\delta\omega_w}$ are chosen according to (58), and the

parameters, $f_{\psi/\delta\omega_0}$, $w_{\psi/\delta\omega_0}$, and $m_{\psi/\delta\omega_0}$, are chosen according to (60); see Table 1. The value for the standard deviation of the orientation bias, σ_{ψ_0}, reflects aided calibration of the attitude angles and is somewhat more conservative than reported in Grejner-Brzezinska et al. (1998).

The gradiometers have errors characterized by red and white noise (Jekeli, 1984, Paik et al., 1997). Again, we start with an idealized model for the corresponding psd:

$$\Phi_{\delta G}(f) = \alpha_{\delta G} f^{-\nu_{\delta G}} + w_{\delta G} \quad , \tag{82}$$

where we abbreviate $\delta G \equiv \delta(\partial a/\partial x)$. The parameters, $\alpha_{\delta G}$, $\nu_{\delta G}$, and $w_{\delta G}$, have positive, given values. We approximate the components in equation (82) with psd models of Type *A*, using parameters, $w_{\delta G}$, $f_{\delta G}$, and $m_{\delta G}$ for the white noise model, and $\alpha_{\delta G}$, f_α, and $\nu_{\delta G}$, for the red noise:

$$\Phi_{\delta G}(f) = \frac{w_\alpha}{\left(1 + \left(\frac{f}{f_\alpha}\right)^2\right)^{m_\nu + \frac{1}{2}}} + \frac{w_{\delta G}}{\left(1 + \left(\frac{f}{f_{\delta G}}\right)^2\right)^{m_{\delta G} + \frac{1}{2}}} \quad , \tag{83}$$

where, according to equation (63):

$$m_\nu = \frac{1}{2}\left(\nu_{\delta G} - 1\right) \quad , \qquad w_\alpha = \alpha_{\delta G} f_\alpha^{-2m_\nu - 1} \quad . \tag{84}$$

VII. Signal Covariance Models

The covariances of the signals (assuming they are stochastic processes) are modeled by first fitting a corresponding analytic psd model (Type *A*) to the observed psd of the signal. For the observed acceleration and angular rate we analyze actual flight data from airborne gravimetry operations. These were obtained, using the periodogram method (with smoothing), from one of the flights of a Twin-Otter aircraft conducted by KMS (Kort & Matrikelstyrelsen / National Survey and Cadastre) of Denmark as part of the Arctic Gravity Project (http://www.nima.mil/GandG/agp/readme.htm). The flight was conducted on 3 August 1999 around the islands of Svalbard and is described in (Jekeli and Kwon, 2001). Figures 2 and 3 show the empirical psd's for $\left(a_1 , a_2 , a_3 \right)$ and $\left(\omega_1 , \omega_2 , \omega_3 \right)$, respectively, as well as the corresponding models of the form

$$\Phi(f) = \frac{c1}{\left(1 + \left(\frac{f}{f1_c} \right)^2 \right)^{m1 + 1/2}} + \frac{c2}{\left(1 + \left(\frac{f}{f2_c} \right)^2 \right)^{m2 + 1/2}} \quad . \tag{85}$$

Values for the constants, c_1, c_2, $f1_c$, $f2_c$, $m1$, $m2$, are shown in Table 2. In all cases, the very-high frequency dynamics (vibrations at frequencies greater than 10 Hz), are not modeled under the assumption that these would be filtered from the data by appropriate smoothing.

These models for the aircraft accelerations do not include the constant accelerations sensed by the accelerometers which account for the reactions to Coriolis, centrifugal, and gravitational accelerations. If an airplane is flying straight and level at constant velocity, the navigation equations in the local NED frame and in spherical approximation (Jekeli, 2000, p.129) yield the following sensed accelerations, since in this case, $dv_N/dt = 0$, $dv_E/dt = 0$, and $v_D = 0$:

$$\begin{aligned}
a_N^0 &= \left(2\omega_e + \frac{v_E}{(R+h)\cos\phi} \right) v_E \sin\phi - g_N , \\
a_E^0 &= \left(2\omega_e + \frac{v_E}{(R+h)\cos\phi} \right) v_N \sin\phi - g_E , \\
a_D^0 &= 2\omega_e v_E \cos\phi + \frac{v_E^2 + v_N^2}{R+h} - - g_D ,
\end{aligned} \tag{86}$$

where ω_e is Earth's spin rate; v_N and v_E are north and east velocities; R is Earth's mean radius; (ϕ, λ, h) are latitude, longitude, and height of the airplane; and (g_N, g_E, g_D) are the north, east,

and down gravity components. The most significant term in these equations is $g_D \approx 9.8\ \mathrm{m/s}^2$. Next in importance are the terms with $\omega_e \approx 7.292 \times 10^{-5}$ rad/s, of the order, $O\left(5 \times 10^{-3}\ \mathrm{m/s}^2\right)$. These nominal values can be substantially larger if the instrument is not level, which was the case for the strapdown unit on the Svalbard flight, resulting in

$$\left(\boldsymbol{a}^b\right)^0 = C_n^b \left(\boldsymbol{a}^n\right)^0 . \tag{87}$$

If the tilt of the "horizontal" accelerometers is $6°$, more than $1\ \mathrm{m/s}^2$ from the vertical gravity couples to their output.

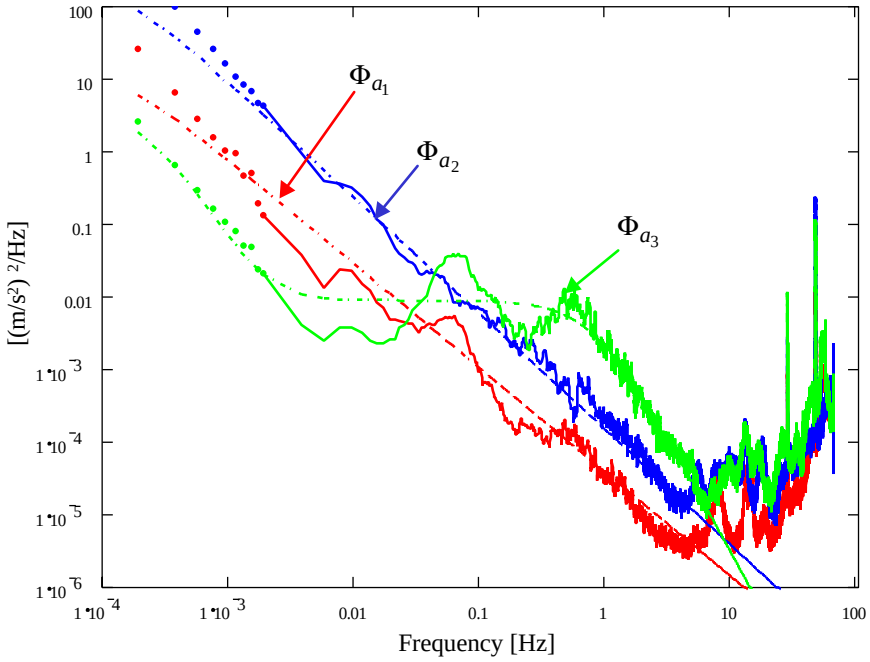

Figure 2: Psd's of body-frame accelerations, $\left(a_1, a_2, a_3\right)$, of Twin-Otter aircraft. Dots: unsmoothed psd; solid line: median-smoothed psd; dashed line: model psd.

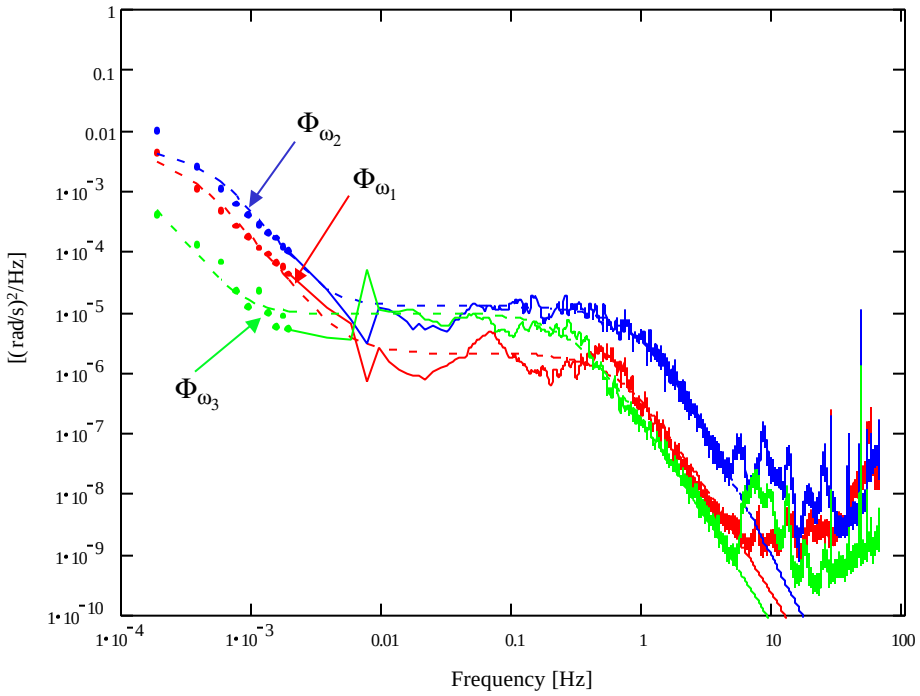

Figure 3: Psd's of body-frame angular rates, $\left(\omega_1, \omega_2, \omega_3\right)$, of Twin-Otter aircraft. Dots: unsmoothed psd; solid line: median-smoothed psd; dashed line: model psd.

Therefore, we write for the acceleration

$$\boldsymbol{a} = \boldsymbol{a}^0 + \Delta\boldsymbol{a} \quad . \tag{88}$$

The covariance functions for the accelerations, thus, more properly are correlation functions:

$$\begin{aligned} \phi_a(\tau) = \left(a^0\right)^2 &+ \frac{2\, c1\, f1_c\sqrt{\pi}}{\Gamma\left(m1+\frac{1}{2}\right)} \left(\pi f1_c\, \tau\right)^{m1} K_{m1}\left(2\pi f1_c \tau\right) \\ &+ \frac{2\, c2\, f2_c\sqrt{\pi}}{\Gamma\left(m2+\frac{1}{2}\right)} \left(\pi f2_c\, \tau\right)^{m2} K_{m2}\left(2\pi f2_c \tau\right) . \end{aligned} \tag{89}$$

Values of a_1^0, a_2^0, and a_3^0 for the Svalbard flight are also given in Table 2.

Then, for the gravity estimation error psd's, equations (72) and (73), the component for the

product of orientation error and acceleration is given by the Fourier transform of the covariance, $\phi_\psi \phi_a$:

$$\mathsf{F}^{-1}\left(\boldsymbol{\Phi}_{\psi a}\right) = \phi_\psi \, \phi_a = \left(\phi_{\psi/\delta\omega_0} + \phi_{\psi/\delta\omega_w} + \phi_{\psi_0}\right)\left(\phi_{a^0} + \phi_{\Delta a}\right) \quad , \tag{90}$$

where the first term is given by equation (81) and the second term is given by equation (89). Expanding, we have

$$\phi_\psi \, \phi_a = \sigma^2_{a^0}\left(\phi_{\psi/\delta\omega_0} + \phi_{\psi/\delta\omega_w} + \phi_{\psi_0}\right) + \phi_{\Delta a}\left(\phi_{\psi/\delta\omega_0} + \phi_{\psi/\delta\omega_w} + \sigma^2_{\psi_0}\right) \quad , \tag{91}$$

meaning that psd's need to be computed numerically only for the products, $\phi_{\Delta a}\,\phi_{\psi/\delta\omega_0}$ and $\phi_{\Delta a}\,\phi_{\psi/\delta\omega_w}$. All other psd's are the analytic models scaled by either $\sigma^2_{a^0}$ or $\sigma^2_{\psi_0}$.

Similarly, for the gradient estimation error psd's, equations (74) and (75), the form of each element is given by

$$\phi_\Gamma \, \phi_\psi = \left(\phi_{\Gamma^0} + \phi_{\Delta\Gamma}\right)\left(\phi_{\psi/\delta\omega_0} + \phi_{\psi/\delta\omega_w} + \phi_{\psi_0}\right) \quad , \tag{92}$$

where Γ^0 is the nominal gravitational gradient element (non-zero only for the in-line gradients, with values corresponding to a mean spherical Earth; see Table 3). Expanding, we find

$$\phi_\Gamma \, \phi_\psi = \sigma^2_{\Gamma^0}\left(\phi_{\psi/\delta\omega_0} + \phi_{\psi/\delta\omega_w} + \phi_{\psi_0}\right) + \phi_{\Delta\Gamma}\left(\phi_{\psi/\delta\omega_0} + \phi_{\psi/\delta\omega_w} + \sigma^2_{\psi_0}\right) \quad , \tag{93}$$

which requires numerical psd's only for the products, $\phi_{\Delta\Gamma}\,\phi_{\psi/\delta\omega_0}$ and $\phi_{\Delta\Gamma}\,\phi_{\psi/\delta\omega_w}$. Finally, we also need numerical psd's for the product, $\phi_\omega \, \phi_{\delta\omega_w}$, in the error covariance component

$$\phi_\omega \, \phi_{\delta\omega} = \phi_\omega\left(\phi_{\delta\omega_0} + \phi_{\delta\omega_w}\right) = \phi_\omega\left(\sigma^2_{\delta\omega_0} + \phi_{\delta\omega_w}\right) \quad . \tag{94}$$

The along-track psd models for the gravitational gradients were obtained as follows. First, (auto-) covariance models for the gravitational gradients (with respect to a reference field) were expressed in terms of a covariance model for the disturbing potential, each gradient model being a linear combination, as in equation (66), respectively, of equations (B-34), (B-37), (B-39), (B-44), (B-46), or (B-48). Parameters for these models, in turn, were selected on the basis of a fit to the 2-D, azimuth-averaged empirical psd for the gravity disturbance, derived from the psd for the global potential model, EGM96 (Lemoine et a., 1998), from $1' \times 1'$ mean gravity anomaly data in the U.S., and from $30'' \times 30''$ and $1'' \times 1''$ elevation data in the U.S. (the latter two by the periodogram method). Both rough and smooth areas could be considered and would yield

different psd models. A moderately rough are was selected for these studies (Montana / Wyoming area). Equation (36) provides the relationship between the psd's of the gravity disturbance and elevation (at high spatial frequencies the gravity anomaly and gravity disturbance are practically identical). Figure 4 shows the empirical psd's and the model constructed therefrom, with corresponding parameter values given in Table 3.

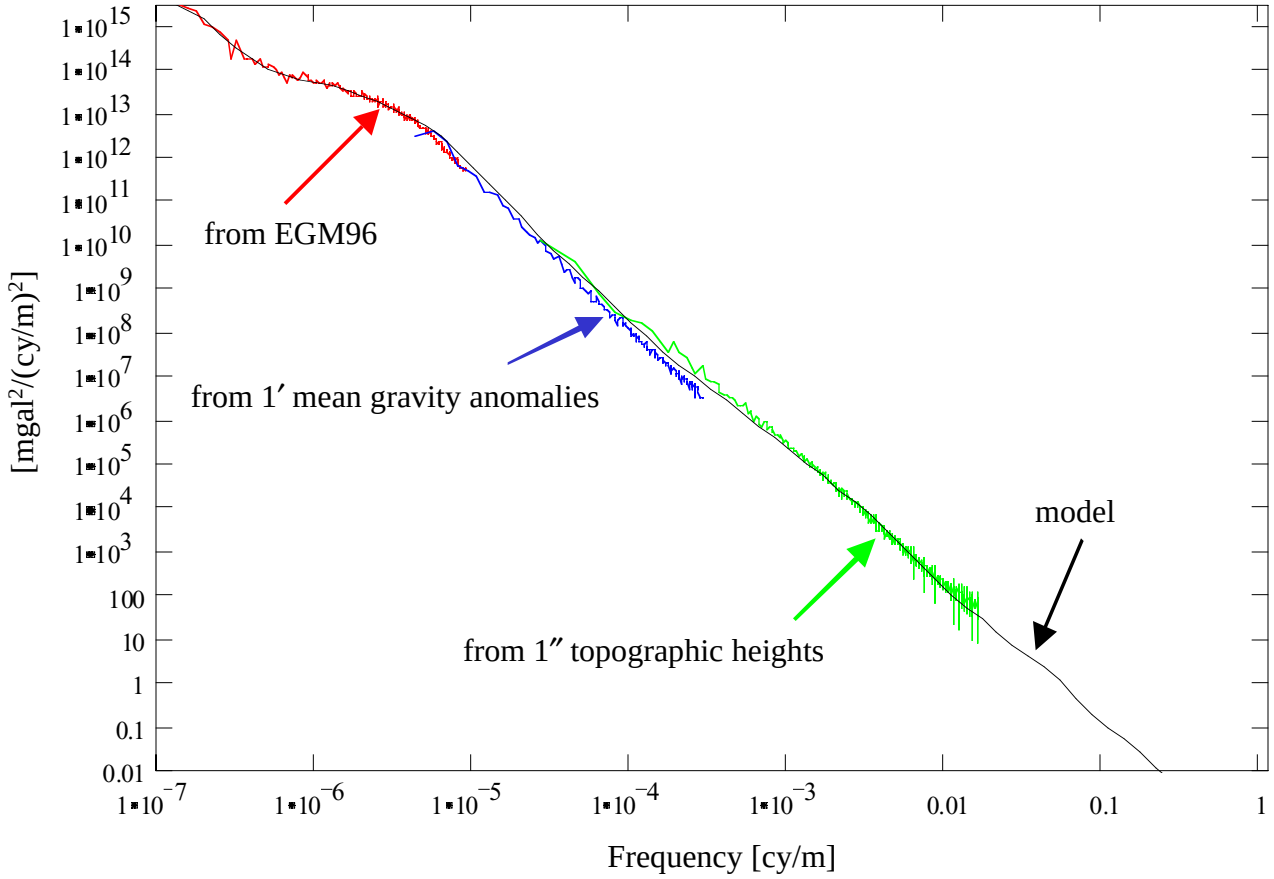

Figure 4: Psd of the vertical gravitational acceleration signal from various data sets, as indicated, plus a fitted model.

The independent variable in these cases is the relative distance, and, in order to convert this to the time variable, we assume that the vehicle is moving with constant velocity, v:

$$v = \frac{s}{\tau} \quad . \tag{95}$$

The along-track gradient covariances are evaluated at points along the track using $s = v\tau$.

Subsequently, the numerically determined Fourier transforms of the covariance products, $\phi_{\Delta\Gamma}\phi_{\psi/\delta\omega_0}$ and $\phi_{\Delta\Gamma}\phi_{\psi/\delta\omega_w}$, are along-track (1D) psd's.

When comparing the along-track error psd's (corresponding to the transforms of equation (72) through (75)), to the along-track psd's of the total gravitational signal, we also need a transformation from the spatial frequency domain to the temporal frequency domain. In this case the models listed in Appendix C are utilized with the appropriate parameters and converted under the assumption of constant velocity:

$$\Phi(f) = \frac{1}{v}\, S\left(\frac{1}{v}\, f\right) \ , \tag{96}$$

where f is the temporal frequency.

Table 1: Values of model parameters for the instrument error psd's.

Error Component	Parameters			equ.
kin. acceleration err.:				(76)
position white noise	$\sigma_{\delta x} = 0.1$ m ,	$\tau_{\delta x} = 1$ s ,	$m_{\delta x} = 10$	
accelerometer error:				(77)
white noise	$\sigma_{\delta a} = 25$ mgal ,	$\tau_{\delta a} = 1$ s ,	$m_{\delta a} = 10$	
gyro rate error:				(80)
bias repeatability	$\sigma_{\delta\omega_0} = 0.003$ °/hr ,	$\tau_{\delta\omega_0} = 7200$ s ,	$m_{\delta\omega_0} = 10$	
white noise	$\sqrt{w_{\delta\omega_w}} = 0.06$ °/hr/$\sqrt{\text{Hz}}$,	$f_{\delta\omega_w} = 10$ Hz ,	$m_{\delta\omega_w} = 10$	
orientation error:				(81)
bias	$\sigma_{\psi_0} = 0.005$ ° ,	$\tau_{\psi_0} = 7200$ s ,	$m_{\psi_0} = 10$	
due to $\delta\omega_w$	$w_{\psi/\delta\omega_w} \equiv w = w_{\delta\omega_w}/(2\pi f_c)^2$,	$f_{\psi/\delta\omega_w} \equiv f_c = 10^{-5}$ Hz ,	$m_{\psi/\delta\omega_w} = 0.5$	(58)
due to $\delta\omega_0$	$w_{\psi/\delta\omega_0} \equiv w =$ eq.(60) ,	$f_{\psi/\delta\omega_0} \equiv f_c = (\tau_{\delta\omega_0}{*}1.15)^{-1}$,	$m_{\psi/\delta\omega_0} = m_{\delta\omega_0} + 1$	(60)
gradiometer error:				(83)
white noise	$\sqrt{w_{\delta G}} = 30$ E/$\sqrt{\text{Hz}}$,	$f_{\delta G} = 10$ Hz ,	$m_{\delta G} = 10$	
red noise*	$\alpha_{\delta G} = 1.7\times10^{-4}$,	$f_\alpha = 10^{-5}$ Hz ,	$\nu_{\delta G} = 1.6$	(84)

* parameter values yield units for psd: E^2/Hz .

Table 2: Values of model parameters for vehicle dynamics psd's.

Dynamics	Parameters	equ.
vehicle acceleration psd	$c1_{a1} = 12\ (\mathrm{m/s^2})^2/\mathrm{Hz}$, $f1_{c_{a1}} = 1.5\times10^{-4}$ Hz, $m1_{a1} = 0.22$, $c2_{a1} = 0\ (\mathrm{m/s^2})^2/\mathrm{Hz}$; $c1_{a2} = 190\ (\mathrm{m/s^2})^2/\mathrm{Hz}$, $f1_{c_{a2}} = 1.5\times10^{-4}$ Hz, $m1_{a2} = 0.3$, $c2_{a2} = 0\ (\mathrm{m/s^2})^2/\mathrm{Hz}$; $c1_{a3} = 4\ (\mathrm{m/s^2})^2/\mathrm{Hz}$, $f1_{c_{a3}} = 2.2\times10^{-4}$ Hz, $m1_{a3} = 0.85$, $c2_{a3} = 0.009\ (\mathrm{m/s^2})^2/\mathrm{Hz}$, $f2_{c_{a3}} = 0.8$ Hz, $m2_{a3} = 1.1$.	(85)
nominal vehicle accelerations	$a_1^0 = 1.3282\ \mathrm{m/s^2}$, $a_2^0 = 1.0344\ \mathrm{m/s^2}$, $a_3^0 = 9.6715\ \mathrm{m/s^2}$.	(86)
vehicle angular rate psd	$c1_{\omega1} = 0.005\ (\mathrm{rad/s})^2/\mathrm{Hz}$, $f1_{c_{\omega1}} = 3\times10^{-4}$ Hz, $m1_{\omega1} = 0.85$, $c2_{\omega1} = 2.2\times10^{-6}\ (\mathrm{rad/s})^2/\mathrm{Hz}$, $f2_{c_{\omega1}} = 0.7$ Hz, $m2_{\omega1} = 1.25$; $c1_{\omega2} = 0.005\ (\mathrm{rad/s})^2/\mathrm{Hz}$, $f1_{c_{\omega2}} = 5\times10^{-4}$ Hz, $m1_{\omega2} = 1$, $c2_{\omega2} = 1.3\times10^{-5}\ (\mathrm{rad/s})^2/\mathrm{Hz}$, $f2_{c_{\omega2}} = 1$ Hz, $m2_{\omega2} = 1.6$; $c1_{\omega3} = 0.005\ (\mathrm{rad/s})^2/\mathrm{Hz}$, $f1_{c_{\omega3}} = 1\times10^{-4}$ Hz, $m1_{\omega3} = 1$, $c2_{\omega3} = 1.\times10^{-5}\ (\mathrm{rad/s})^2/\mathrm{Hz}$, $f2_{c_{\omega3}} = 0.3$ Hz, $m2_{\omega3} = 1.2$.	(85)

Table 3: Values of model parameters for the gravitational field.

	Parameters	equ.
disturbing potential psd (spatial frequencies)	$\sigma_1^2 = 1\times10^5\ \mathrm{m^2/s^2}$, $\alpha_1 = 3\times10^{-7}\ \mathrm{m^{-1}}$, $\sigma_2^2 = 3500\ \mathrm{m^2/s^2}$, $\alpha_2 = 7.7\times10^{-7}\ \mathrm{m^{-1}}$, $\sigma_3^2 = 778\ \mathrm{m^2/s^2}$, $\alpha_3 = 3\times10^{-6}\ \mathrm{m^{-1}}$, $\sigma_4^2 = 300\ \mathrm{m^2/s^2}$, $\alpha_4 = 8.5\times10^{-6}\ \mathrm{m^{-1}}$, $\sigma_5^2 = 20\ \mathrm{m^2/s^2}$, $\alpha_5 = 2\times10^{-5}\ \mathrm{m^{-1}}$, $\sigma_6^2 = 0.3\ \mathrm{m^2/s^2}$, $\alpha_6 = 6\times10^{-5}\ \mathrm{m^{-1}}$, $\sigma_7^2 = 0.03\ \mathrm{m^2/s^2}$, $\alpha_7 = 1.2\times10^{-4}\ \mathrm{m^{-1}}$, $\sigma_8^2 = 0.003\ \mathrm{m^2/s^2}$, $\alpha_8 = 2\times10^{-4}\ \mathrm{m^{-1}}$, $\sigma_9^2 = 5\times10^{-4}\ \mathrm{m^2/s^2}$, $\alpha_9 = 5\times10^{-4}\ \mathrm{m^{-1}}$, $\sigma_{10}^2 = 4\times10^{-5}\ \mathrm{m^2/s^2}$, $\alpha_{10} = 1.2\times10^{-3}\ \mathrm{m^{-1}}$, $\sigma_{11}^2 = 3\times10^{-6}\ \mathrm{m^2/s^2}$, $\alpha_{11} = 3\times10^{-3}\ \mathrm{m^{-1}}$, $\sigma_{12}^2 = 3\times10^{-7}\ \mathrm{m^2/s^2}$, $\alpha_{12} = 6.5\times10^{-3}\ \mathrm{m^{-1}}$, $\sigma_{13}^2 = 8\times10^{-9}\ \mathrm{m^2/s^2}$, $\alpha_{13} = 1.9\times10^{-2}\ \mathrm{m^{-1}}$ $\sigma_{14}^2 = 4.4\times10^{-10}\ \mathrm{m^2/s^2}$, $\alpha_{14} = 6\times10^{-2}\ \mathrm{m^{-1}}$, $\sigma_{15}^2 = 8.6\times10^{-12}\ \mathrm{m^2/s^2}$, $\alpha_{15} = 2.1\times10^{-1}\ \mathrm{m^{-1}}$, $\sigma_{16}^2 = 1.5\times10^{-13}\ \mathrm{m^2/s^2}$, $\alpha_{16} = 8\times10^{-1}\ \mathrm{m^{-1}}$	(66) $J = 16$
nominal gravitational gradients	$\Gamma^0_{1,1} = 1540$ E, $\Gamma^0_{2,2} = 1540$ E, $\Gamma^0_{3,3} = 3080$ E	
velocity to convert to temporal psd's	$v = 250$ km/hr	(96)
altitude of aircraft	$x_3 = 1000$ m	(66)

VIII. Airborne Gravimetry Error Analysis

Based on typical parameter values for the errors in high-accuracy gyros and orientation bias (Table 1), and the acceleration spectral densities and mean signal amplitudes (Table 2), Figures 5 through 8 show the contributions from the orientation error due to the coupling between gyro error and aircraft dynamics (acceleration) according to equation (90). In Figure 5, for $F_{y_3 a_2}$, we see that the dominant contributors are the coupling between an azimuth bias, y_3^0, and the horizontal (east, in this case) aircraft acceleration at all frequencies. At lower frequencies, the coupling of the azimuth bias with the mean amplitude of the horizontal acceleration raises the error psd significantly. The latter contribution extends to the mid-frequencies (0.0003 Hz) only because the psd of the bias is modeled with a time constant of 2 hr; a longer time constant would move the amplification to even lower frequencies.

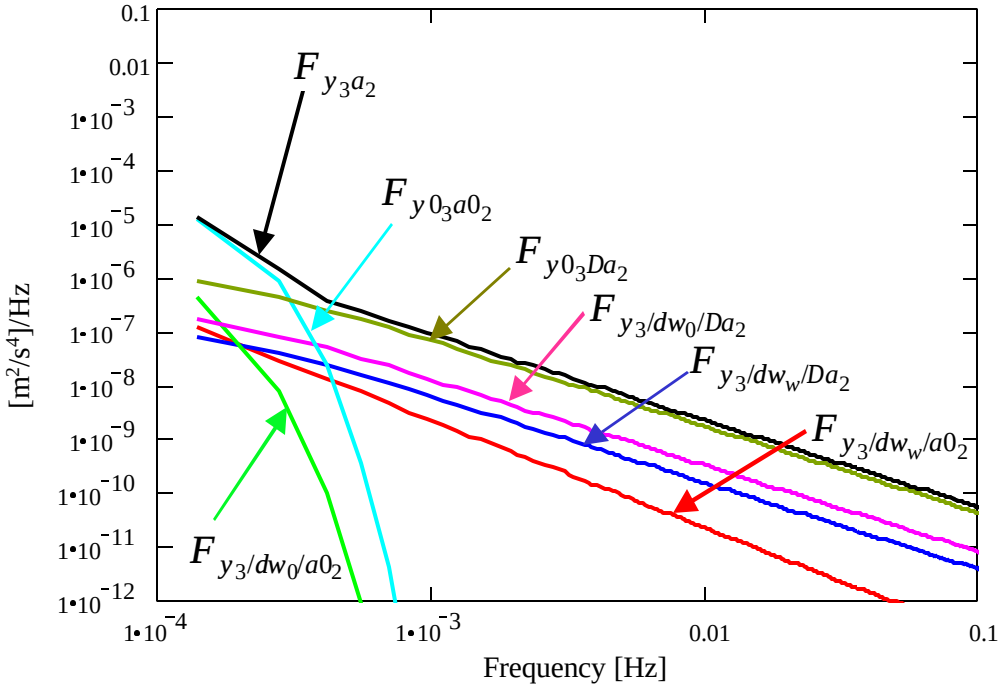

Figure 5: Psd of down orientation error, y_3, due to gyro error coupling with east acceleration, a_2.

It is also seen that all other components contribute about one order of magnitude less to the orientation error psd. An increase of the gyro bias variance from $(0.003\ °/\text{hr})^2$ to $(0.01\ °/\text{hr})^2$ would yield an equivalent level of error. Similarly, the white noise psd of the gyro must increase by a factor of 10 to be commensurate with the azimuth bias variance. Yet, the assumed initial value of this variance, $(0.005°)^2$, is low compared to typical calibration using standard initial alignment procedures by an inertial navigation system (INS) (we assume a more accurate

calibration en route using GPS). A less well-calibrated azimuth bias would make the gyro errors even less important to this part of the overall error. These relationships between contributions to orientation error from azimuth bias and gyro error are largely independent of the spectrum of the horizontal acceleration of the aircraft; but the accelerations obviously define the amplitude of the overall high-frequency spectrum of the orientation error.

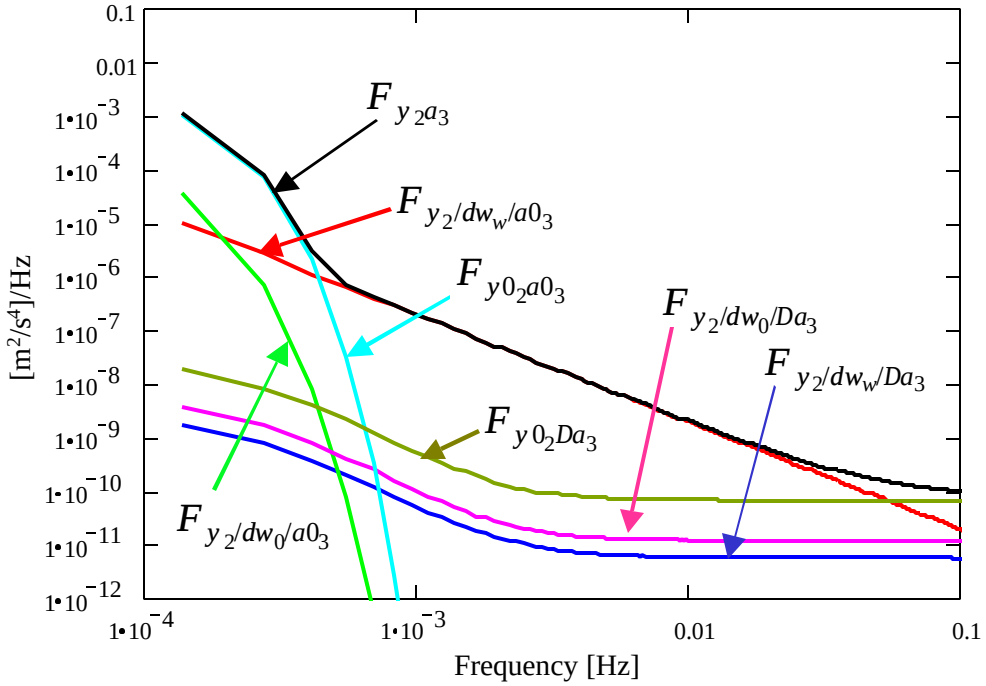

Figure 6: Psd of east orientation error, y_2, due to gyro error coupling with down acceleration, a_3.

The situation is similar for the error psd, $F_{y_2 a_3}$, resulting from the coupling of the gyro error with the down acceleration, with the essential difference, as seen in Figure 6, that the gyro noise, dw_w, now defines the total error at mid frequencies, owing to the large nominal down acceleration of about $9.8\ \mathrm{m/s^2}$. This also elevates the error at the very low frequencies coming from the gyro and orientation biases. Due to the particular spectrum of the vertical acceleration of the aircraft, in this case, the effect of the leveling bias dominates only at the high frequencies (> 0.06 Hz). The same trade-off between the orientation bias, the angular rate bias, and the white noise in the rate exist here as for $F_{y_3 a_2}$.

The latter two error psd's, $F_{y_3 a_2}$ and $F_{y_2 a_3}$, contribute to the error psd of the estimated horizontal gravity, while those shown in Figures 7 and 8, $F_{y_2 a_1}$ and $F_{y_1 a_2}$, contribute to the error psd of the estimated vertical component. These error psd's and their constituents are very similar to each other and to $F_{y_3 a_2}$.

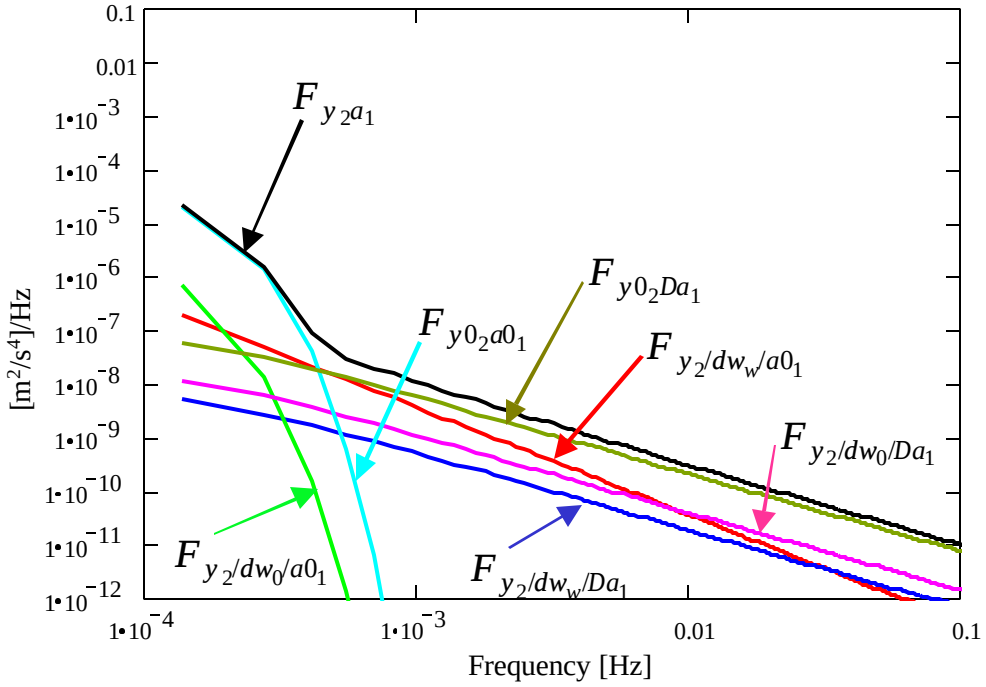

Figure 7: Psd of east orientation error, y_2, due to gyro error coupling with north acceleration, a_1.

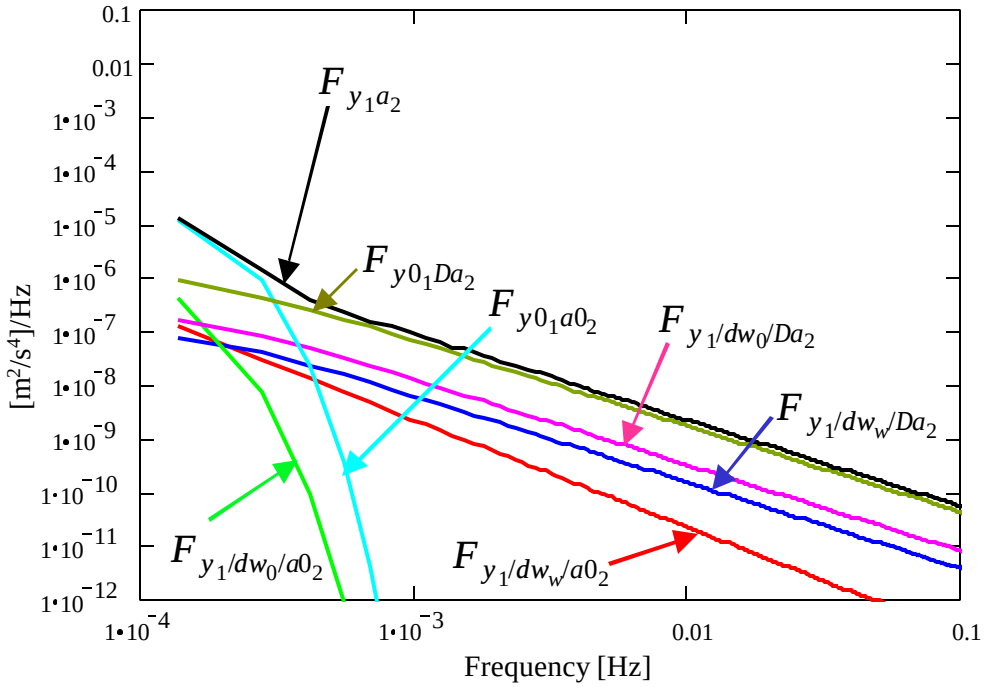

Figure 8: Psd of north orientation error, y_1, due to gyro error coupling with east acceleration, a_2.

Figure 9 shows the constituents of the error psd of the estimated horizontal gravity component. The orientation error contribution, $F_{y_2 a_3}$, dominated by the effect of the large down acceleration, essentially defines the error psd at low- to mid-frequencies. Again, with degradation in the azimuth bias calibration and/or with a more dynamic acceleration environment (higher psd amplitudes), the orientation error contribution, $F_{y_3 a_2}$, would determine to total error psd at these frequencies. At the high frequencies, the white noise amplification resulting from the differentiation of position errors clearly delimits the resolution to which gravity can be recovered. We see the well known spectral window for airborne gravimetry (Schwarz et al., 1992). In this scenario the accelerometer noise psd helps to shape the bottom of the error spectrum, but any improvement in accelerometer noise would not yield a significant overall enhancement. The registration error psd is practically negligible in the presence of accurate positions such as derived from GPS. It is at the level of $F_{G_{11}} s^2_{d x_1} = 1.3 \times 10^{-14}$ m^2/s^4/Hz (not shown in the figure), and would compete with the accelerometer variance only if the latter were reduced by a factor of 5×10^{-6} to about $\left(1.2 \times 10^{-7} \text{ m/s}^2\right)^2$.

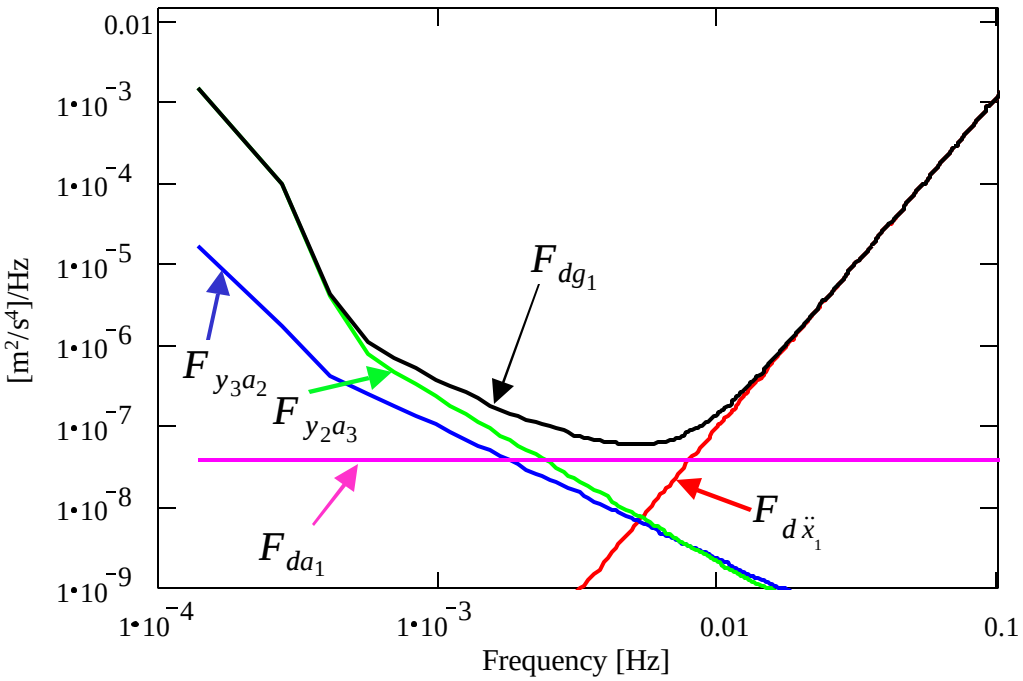

Figure 9: Psd of horizontal gravity estimation error, $d g_1$, due to kinematic acceleration, gyro, and accelerometer errors.

The error psd of the estimated vertical gravity component, shown in Figure 10, has similar characteristics, but is governed by slightly lower orientation error contributions, reflecting

primarily the effect of the lower nominal horizontal acceleration. However, the total acceleration spectrum essentially determines the lower part of the error spectrum. The noise of the accelerometer defines the central frequencies of the overall error spectrum, somewhat more broadly than for the horizontal gravity component.

Figure 11 depicts the total error spectra relative to the along-track psd's of the gravity signal as modeled by the parameters of Table 3 and the functions given by equations (C-7) and (C-12) with $Dx_2 = 0$, and altitude, $x_3 = 1000$ m. As the aircraft velocity (assumed 250 km/hr, here) increases, the along-track psd's of the gravitational signals move to the right with respect to the error psd's. Clearly, the signal-to-error ratio is greater than unity over a broader spectral band in the case of the vertical gravity component, and it is greater than the signal-to-error ratio for the horizontal gravity component. According to the scenario implied by the given error and signal parameters, one can expect better resolution and accuracy in the recovery of the vertical component. Nevertheless, it is also clear that the horizontal component may be estimated with reasonable accuracy (see also Jekeli, 1995).

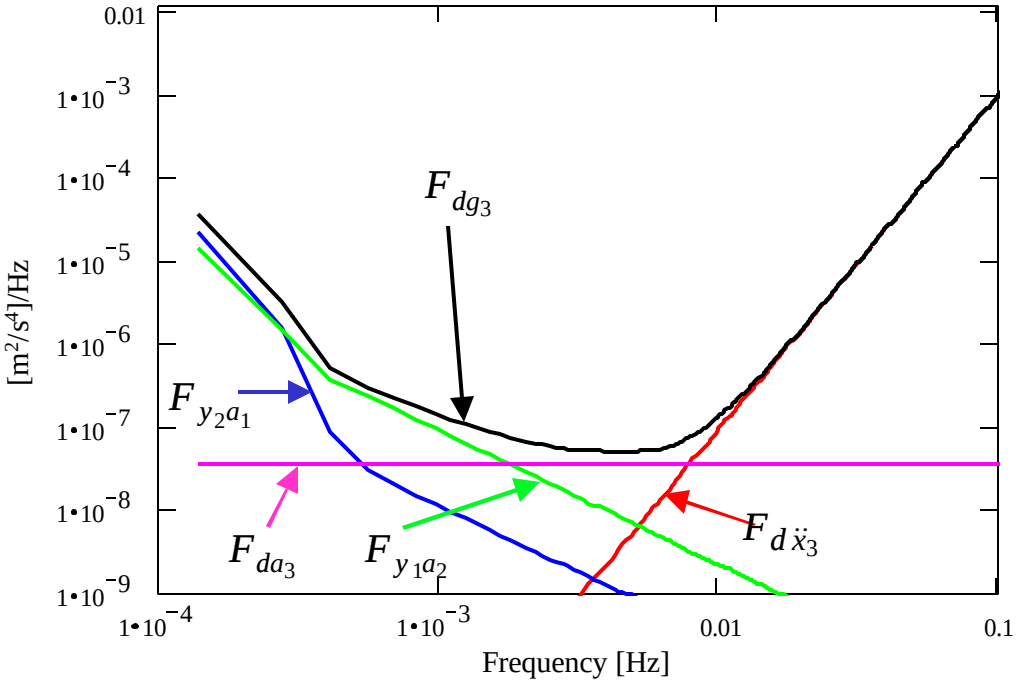

Figure 10: Psd of vertical gravity estimation error, $d g_3$, due to kinematic acceleration, gyro, and accelerometer errors.

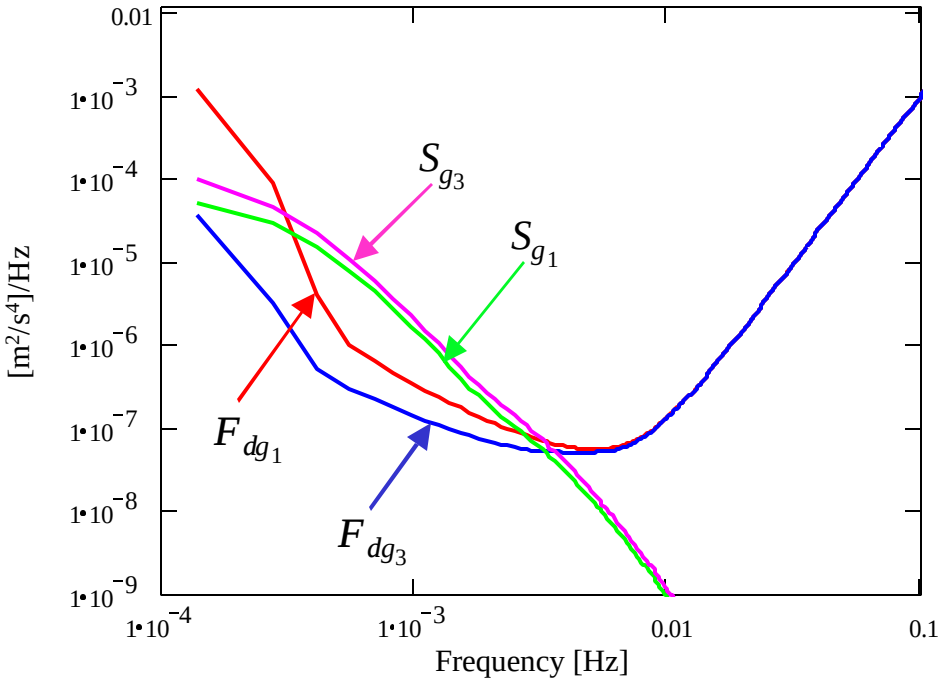

Figure 11: Psd's of gravity estimation errors, $d\,g_1$, $d\,g_3$, versus along-track psd's of corresponding signals.

IX. Airborne Gravity Gradiometry Error Analysis

As background information for the typical gravitational gradients that may be encountered, Figure 12 shows the along-track psd's of the six gradients based on the reciprocal distance model (Table 3) fitted to the empirical data shown in Figure 4. Equations (C-29), (C-32), (C-34), (C-39), (C-41), and (C-43) were used to compute these psd's, with $Dx_2 = 0$, $h = 1000$ m, and $v = 250$ km/hr (see also equation (96)). A gradiometer with $30\ \mathrm{E}/\sqrt{\mathrm{Hz}}$ sensitivity would easily sense gradients with wavelengths as short as 7 km to 17 km. However, due to the attenuation with altitude, more sensitive gradiometers quickly reach the point of diminishing returns. With more than an order of magnitude increased sensitivity, at $1\ \mathrm{E}/\sqrt{\mathrm{Hz}}$, the recoverable wavelengths decrease only to about 1.4 to 2.3 km.

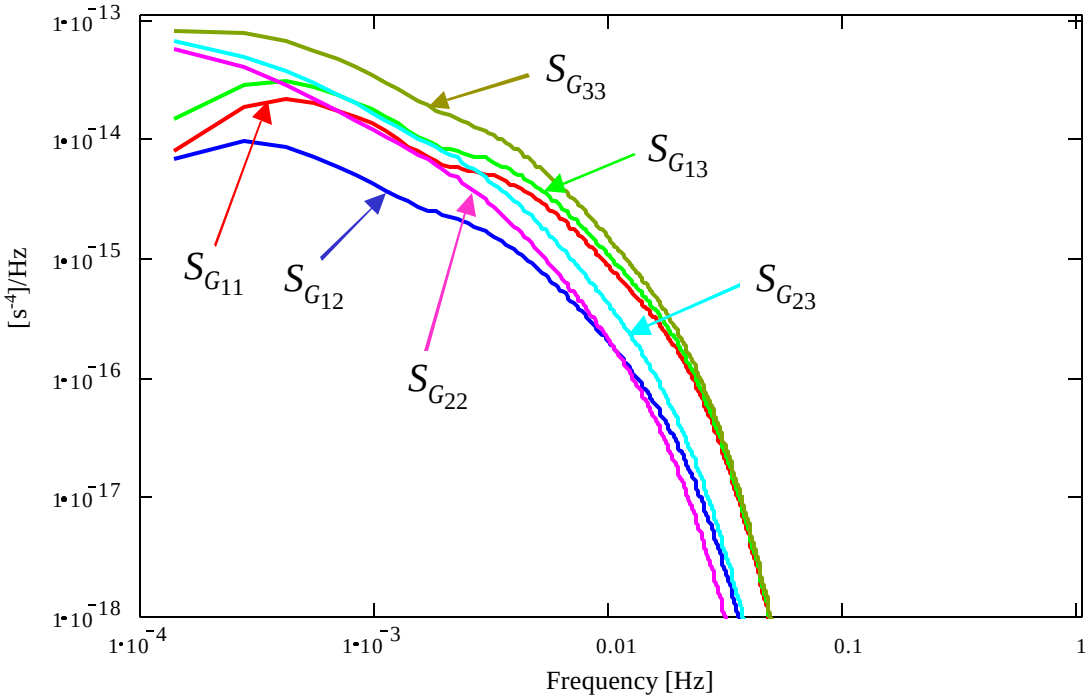

Figure 12: Along-track psd's of gradients at altitude, $h = 1000$ m, and for aircraft with velocity, $v = 250$ km/hr .

We proceed with the error analysis of a full-tensor gradiometer system as described in Section II. Again, based on the nominal parameter values for the gyro errors and orientation bias (Table 1), and the angular rate spectral densities (Table 2), Figures 13 through 18 show the contributions from the orientation error due to the coupling between gyro error and the gradient field, according to equation (92). As before, the orientation errors themselves are due to gyro noise and drift bias, as well as self-bias. Since we assume like values for each of the attitude biases and for the gyro error parameters, the orientation error contributions depend only on the gradient psd's.

Clearly, these gyro and attitude errors contribute more, by several orders of magnitude, in coupling to the in-line gradients (Figures 13 through 15) than in coupling to the cross-gradients

(Figures 16 through 18); and, in either case, primarily the lower frequencies are affected. This is due to the presence of the large nominal in-line gradients. For the cross-gradient couplings, the orientation bias error mostly dominates the contributions. It also dominates for the in-line gradient couplings, but only at the very low frequencies, while at medium and high frequencies, in this case, the coupling of the gyro noise with the nominal gradients defines the overall coupling. On the other hand, degradation in the orientation bias variance by an order of magnitude, from $(0.005\,^\circ)^2$ to $(0.016\,^\circ)^2$, brings its effect to that of the assumed gyro error, as least for the medium frequencies (Figures 13 through 15). This also depends, of course, on the strength of the anomalous gradient field.

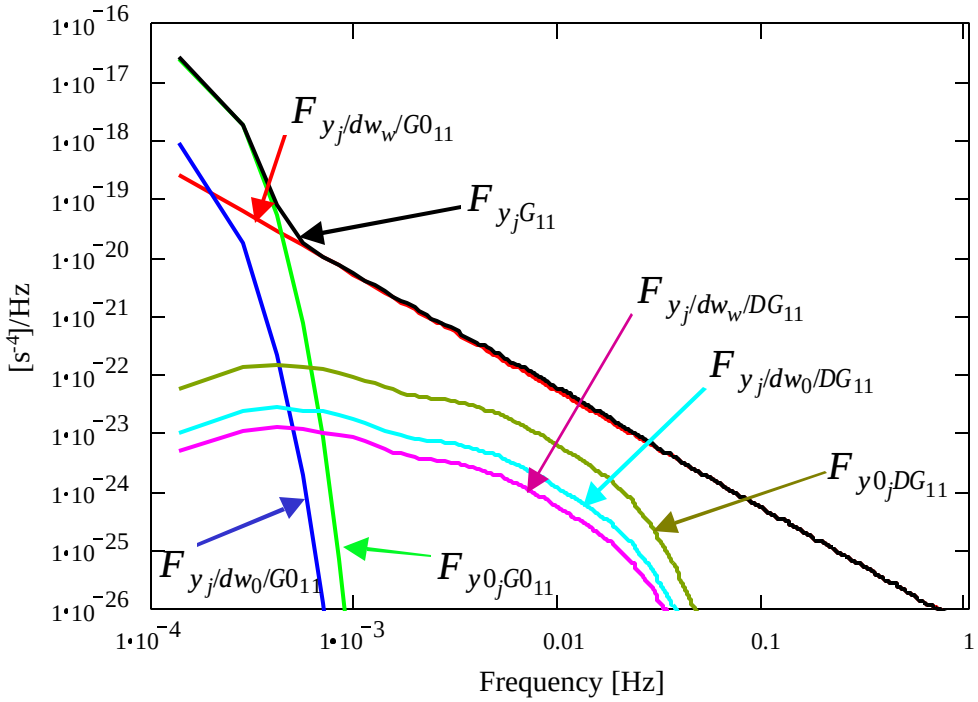

Figure 13: Psd's of errors due to coupling of orientation error, y_j $(j = 2,3)$, with gradient, G_{11} (total psd (black) and its components (colors)).

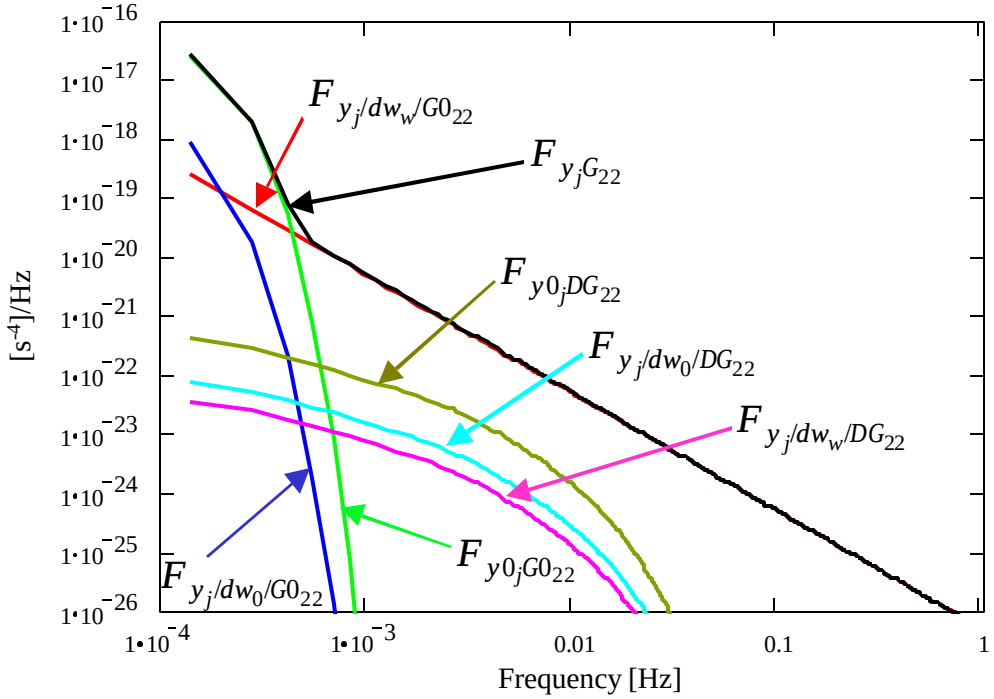

Figure 14: Psd's of errors due to coupling of orientation error, y_j $(j=1,3)$, with gradient, G_{22} (total psd (black) and its components (colors)).

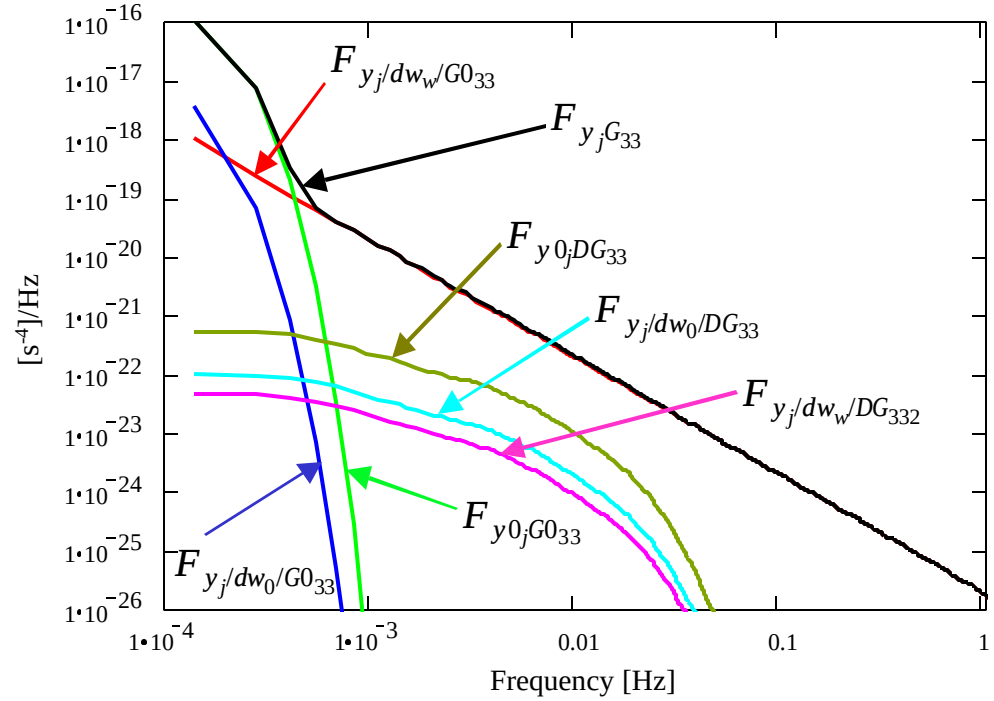

Figure 15: Psd's of errors due to coupling of orientation error, y_j $(j=1,2)$, with gradient, G_{33} (total psd (black) and its components (colors)).

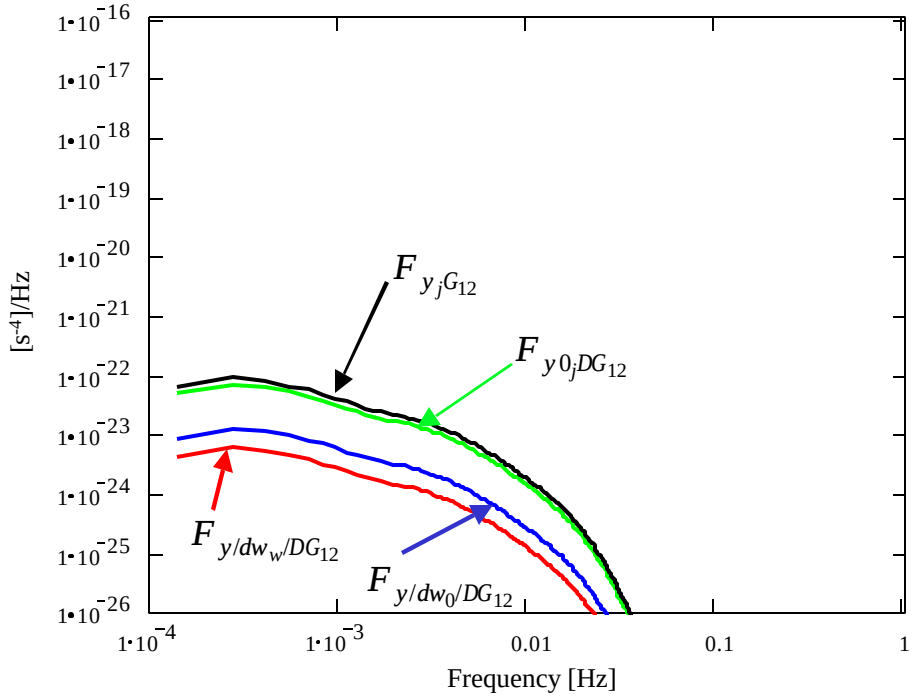

Figure 16: Psd's of errors due to coupling of orientation error, y_j $(j=1,2,3)$, with gradient, G_{12} (total psd (black) and its components (colors)).

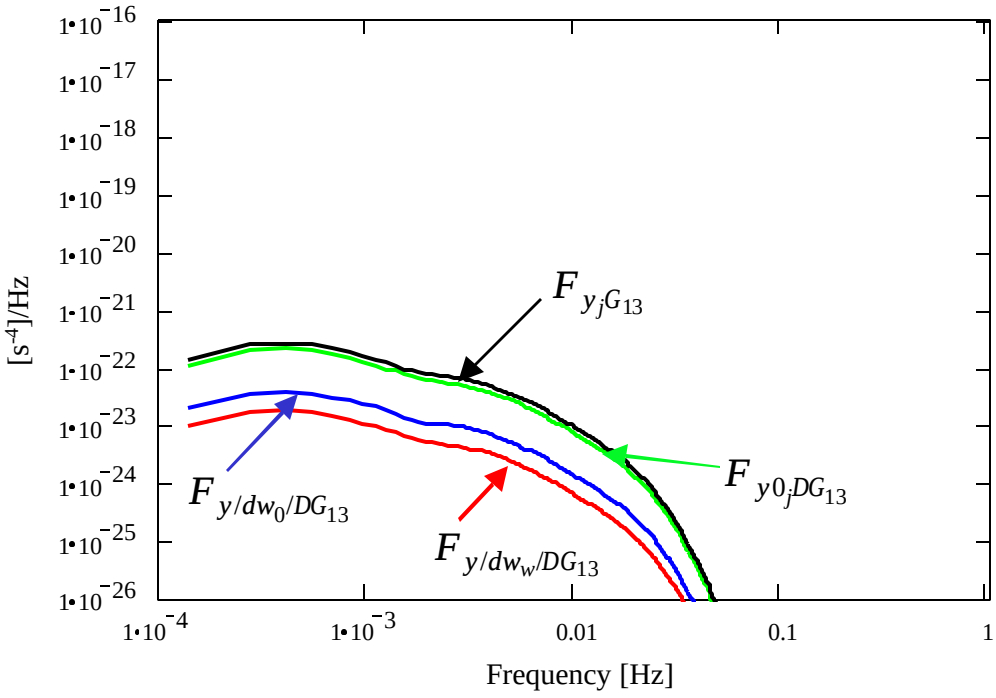

Figure 17: Psd's of errors due to coupling of orientation error, y_j $(j=1,2,3)$, with gradient, G_{13} (total psd (black) and its components (colors)).

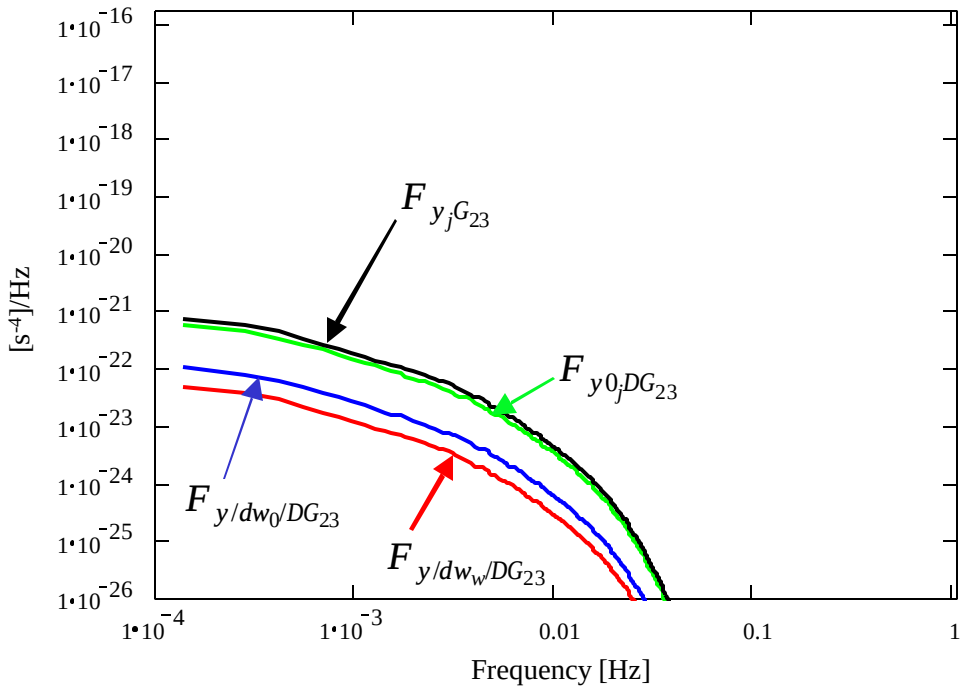

Figure 18: Psd's of errors due to coupling of orientation error, y_j $(j = 1,2,3)$, with gradient, G_{23} (total psd (black) and its components (colors)).

The error psd contributions due to the coupling of the gyro errors, given by equation (78), with the angular dynamics of the vehicle are illustrated in Figure 19. The effect of the white noise dominates over that of the rate biases (medium and high frequencies), and the noise psd would have to decrease by two orders of magnitude to be commensurate with the effect of the rate bias at the medium frequencies. This conclusion is essentially independent of the angular rate dynamics of the vehicle, which couple into both types of gyro error. However, it is also clear that the angular rate dynamics determine the amplitude of all these couplings.

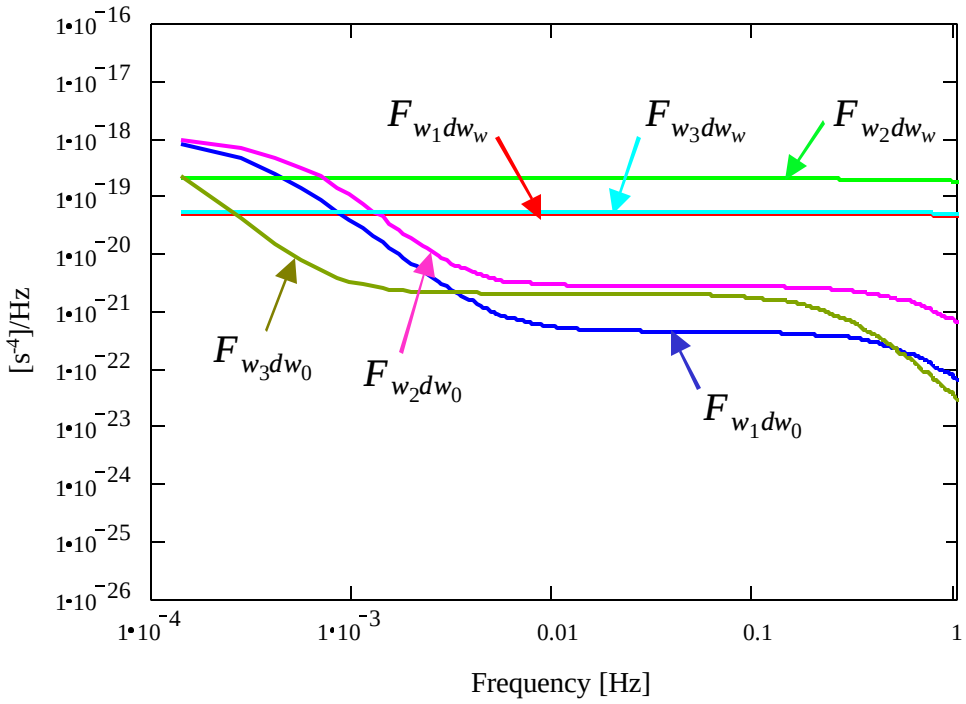

Figure 19: Psd's of errors due to angular rate error, dw .

Finally, Figures 20 through 25 show the combined effects on the error in the computed gradients. For the given values of the error parameters (Table 1), the gradiometer noise determines the error at all frequencies. The next largest contribution is from the couplings of the gyro errors with the angular dynamics of the vehicle; while, the orientation error couplings hardly contribute, except at the low frequencies (due to the orientation bias and nominal in-line gradients), and then only for the cross-gradients since only they are affected by couplings to the in-line gradients. The gyro noise psd's would have to decrease by two to three orders of magnitude before they compete with the gyro error effects, and together they would have to decrease by two to three more orders of magnitude in order to contribute less than the orientation bias effects. Furthermore, the latter affect primarily the low and medium frequencies, whereas the whiteness of the gyro noise essentially contributes equally at all frequencies.

The magnitudes of the various contributing effects essentially depend linearly on the parameter values since the analysis is based on a linear approximation of the error equation. Therefore, one can construct approximate, order-of-magnitude relationships between commensurate levels of gradiometer error, gyro error, and orientation bias (Table 4). Figure 26 shows the psd of the error, dG_{12} , and its constituents for the case of gyro and orientation errors approximately commensurate in effect at the level of $1\ \mathrm{E}/\sqrt{\mathrm{Hz}}$ (the situation is similar for the other gradients). Clearly, in order for the gradiometer error to dominate the accuracy of the derived gravitational gradients, the gyros and orientation bias should be an order of magnitude better in equivalent accuracy. As a final note, all of these results depend on the strength of the gradient field (which is a function of geographic region and aircraft altitude) and the angular rate dynamics of the aircraft.

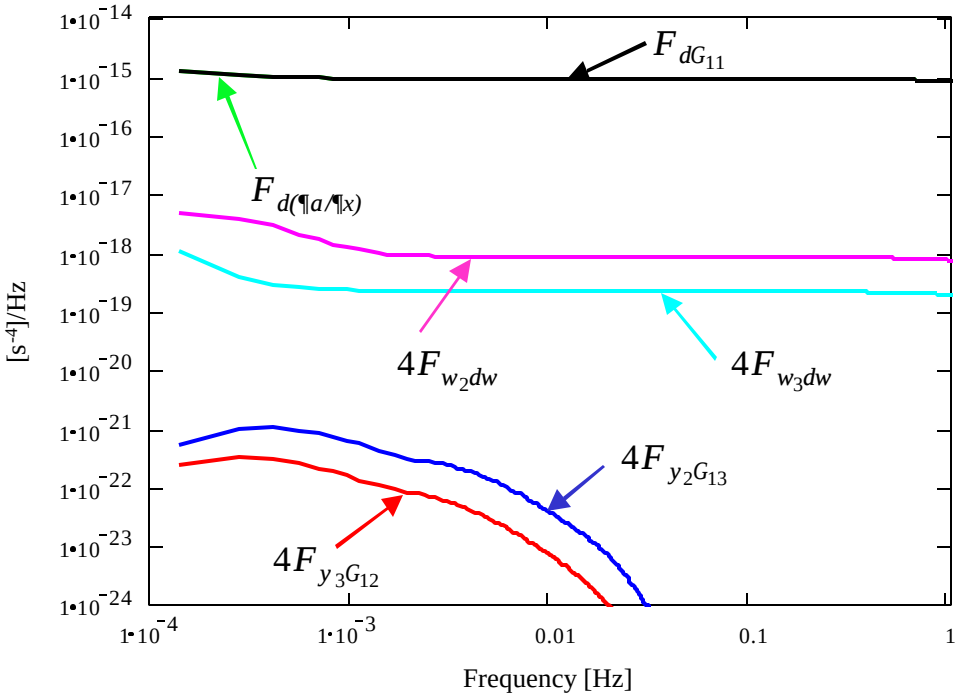

Figure 20: Total psd and its components for the gradient error, dG_{11}.

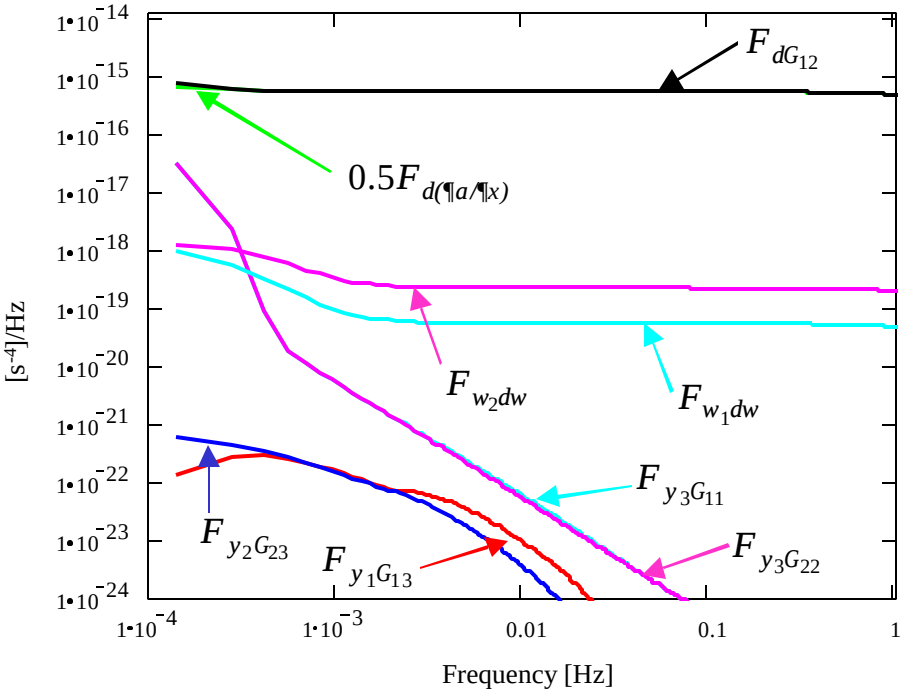

Figure 21: Total psd and its components for the gradient error, dG_{12}.

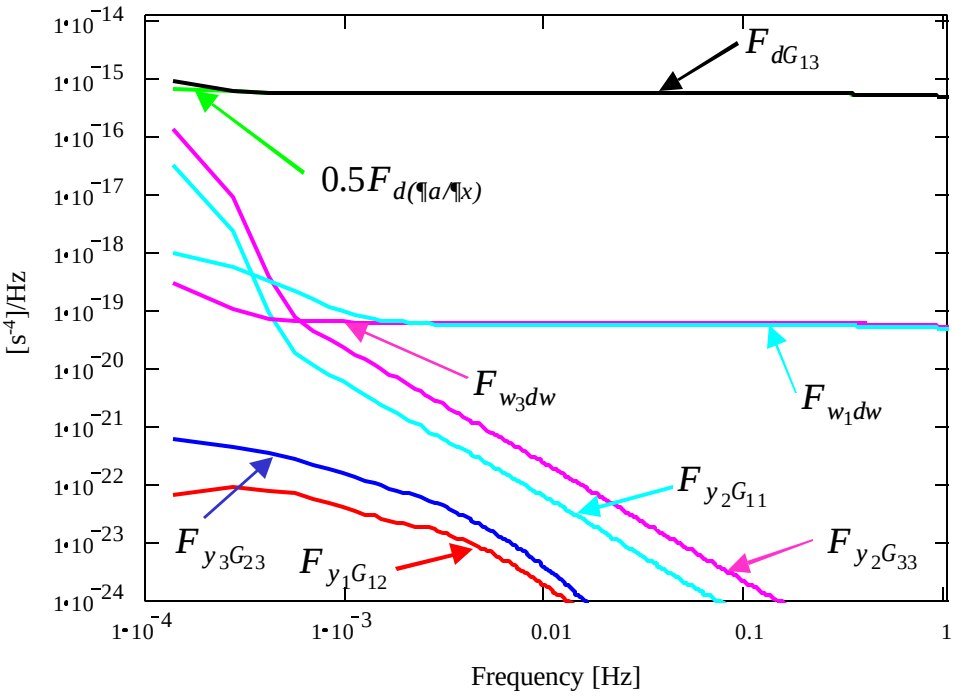

Figure 22: Total psd and its components for the gradient error, dG_{13}.

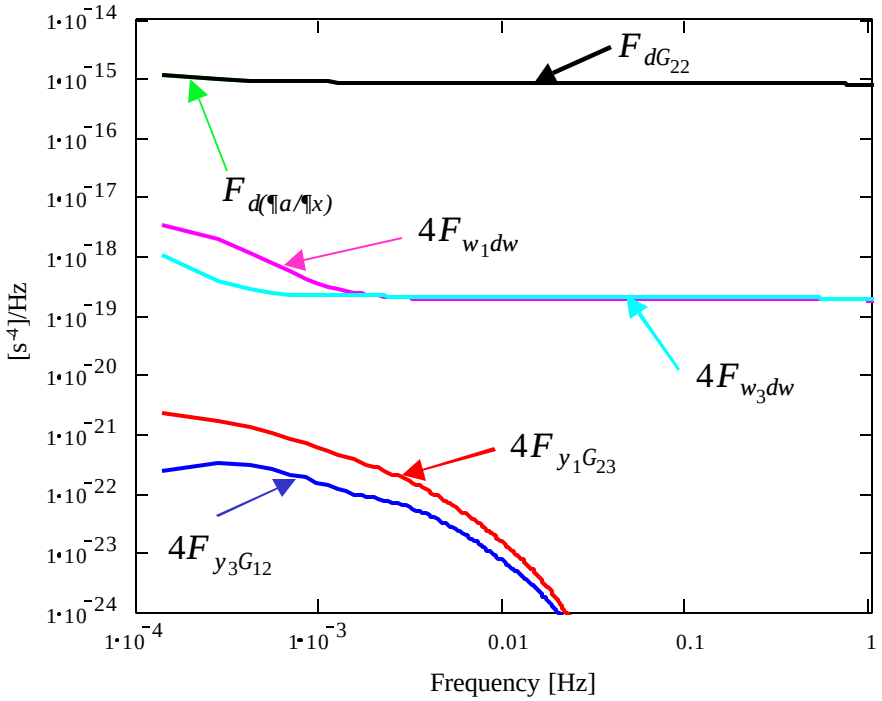

Figure 23: Total psd and its components for the gradient error, dG_{22}.

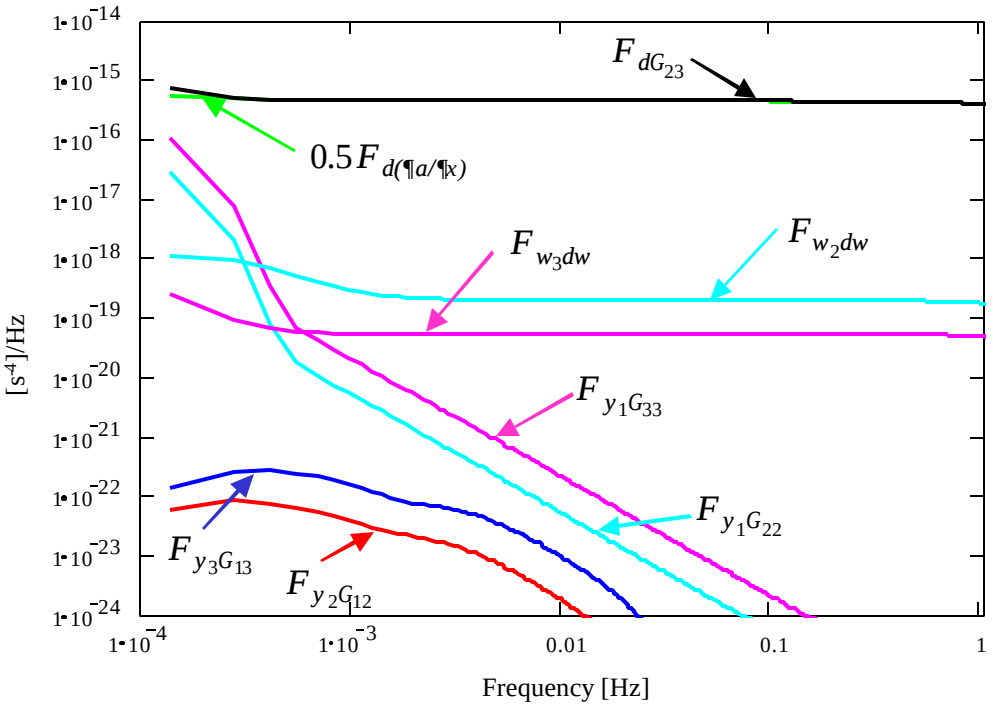

Figure 24: Total psd and its components for the gradient error, dG_{23}.

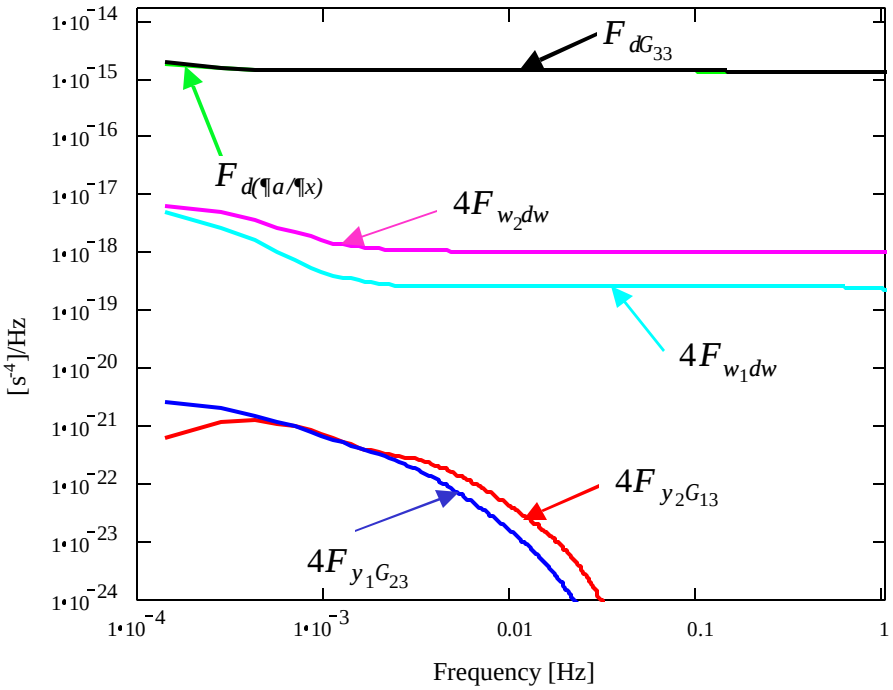

Figure 25: Total psd and its components for the gradient error, dG_{33}.

Table 4: Roughly commensurate sensor errors in airborne gravity gradiometry

$\sqrt{w_{dG}}$, a_{dG} *	s_{y_0}	s_{dw_0}	$\sqrt{w_{dw_w}}$
30 E/$\sqrt{\text{Hz}}$, 5×10^{-2}	20 °	0.5 °/hr	3 °/hr/$\sqrt{\text{Hz}}$
10 E/$\sqrt{\text{Hz}}$, 1.7×10^{-2}	6 °	0.15 °/hr	1 °/hr/$\sqrt{\text{Hz}}$
1 E/$\sqrt{\text{Hz}}$, 1.7×10^{-4}	0.6 °	0.015 °/hr	0.1 °/hr/$\sqrt{\text{Hz}}$
0.1 E/$\sqrt{\text{Hz}}$, 1.7×10^{-6}	0.06 °	0.0015 °/hr	0.01 °/hr/$\sqrt{\text{Hz}}$
0.01 E/$\sqrt{\text{Hz}}$, 1.7×10^{-8}	0.006 °	0.00015 °/hr	0.001 °/hr/$\sqrt{\text{Hz}}$

* units as in Table 1

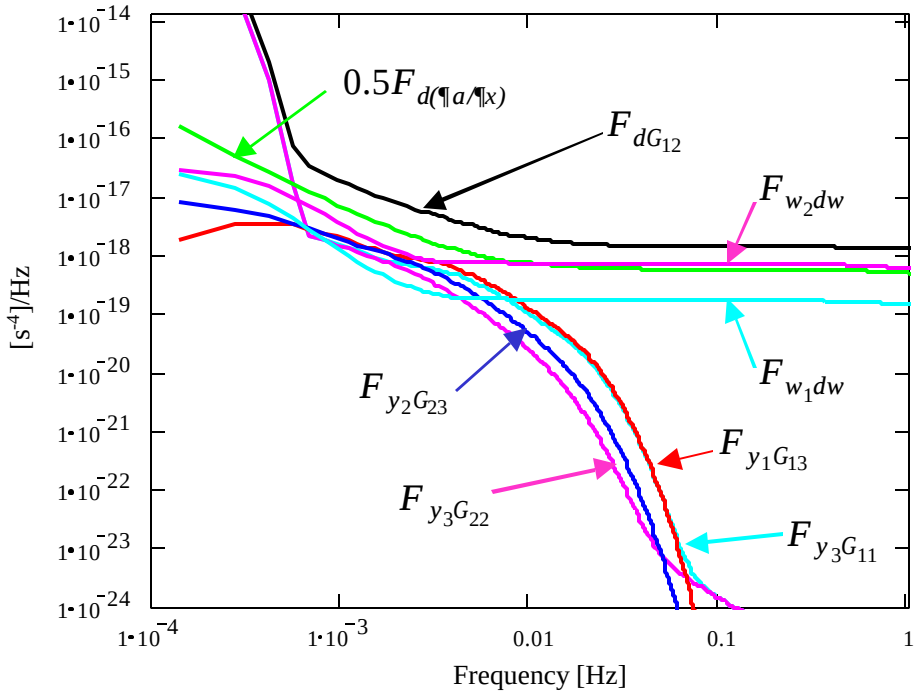

Figure 26: Total psd and its components for the gradient error, dG_{12}, if all constituent error sources are roughly equivalent (third entry in Table 4).

X. Summary

A detailed error analysis in the frequency domain was presented for airborne gravimetry and airborne gravity gradiometry. New psd and covariance models were developed for white noise and the random bias, which can be manipulated analytically to accommodate integration and differentiation of errors and the requirement of stationarity in power spectral densities. Models were also designed for the accelerations and angular rates of an aircraft flying straight and level for survey purposes. Finally gravitational models were derived from actual gravimetric and topographic data in a moderately active geographic region of the U.S. to wavelengths as short as 1 m. Together, these error and signal models predict the recoverable spectral window in airborne gravimetry that is already well known and they highlight the limiting sources of error. Aside from the principal sensor errors, the orientation error bias couples with the accelerations of the aircraft thus bounding the recoverability at the longer wavelengths.

Similarly, in the case of a full tensor gradiometer with the necessary suite of gyros, the coupling of the gyro rate noise to the angular rate environment of the system is the principal competitor to the gradiometer noise. The analysis shows that a gradiometer with $1\,\mathrm{E}\sqrt{\mathrm{Hz}}$ sensitivity will not be adversely compromised (at medium and high frequencies) if the required gyros have bias repeatability of $0.0015\,^\circ/\mathrm{hr}$ and sensitivity of $0.01\,^\circ/\mathrm{hr}/\sqrt{\mathrm{Hz}} \approx 0.00015\,^\circ/\sqrt{\mathrm{hr}}$, and if the orientation bias is $0.06\,^\circ$. The latter numbers all reflect an order of magnitude lower than a commensurate gradient error effect of $1\,\mathrm{E}\sqrt{\mathrm{Hz}}$.

Appendix A

Equation (23) for the error in the gravitational gradients is based on a combination of gradiometer measurements:

$$\delta\Gamma = \Gamma\,\Psi - \Psi\,\Gamma - \delta B + \delta\Omega\,\Omega + \Omega\,\delta\Omega - \sum_j \Xi\,\delta x_j \quad , \tag{A-1}$$

where (see equation (13))

$$B^b = \frac{1}{2}\left(\frac{\partial \boldsymbol{a}^b}{\partial \boldsymbol{x}^b} + \left(\frac{\partial \boldsymbol{a}^b}{\partial \boldsymbol{x}^b}\right)^{\mathrm{T}}\right) \quad . \tag{A-2}$$

Considering only errors in the measurement tensor, $\partial \boldsymbol{a}^b/\partial \boldsymbol{x}^b$, suppose they have a 9×9 variance-covariance matrix that is diagonal (no correlations):

$$\Sigma_{\partial \boldsymbol{a}/\partial \boldsymbol{x}} = \mathrm{diag}\left(\sigma_{jk}^2\right) \quad , \tag{A-3}$$

where σ_{jk}^2 is the variance of the (j,k)-element of $\partial \boldsymbol{a}^b/\partial \boldsymbol{x}^b$. Then, the errors in the gradients can be written as

$$\delta\begin{pmatrix} \Gamma_{1,1} \\ \Gamma_{1,2} \\ \Gamma_{1,3} \\ \Gamma_{2,2} \\ \Gamma_{2,3} \\ \Gamma_{3,3} \end{pmatrix} = \begin{pmatrix} -1 & 0 & 0 & 0 & 0 & 0 & 0 & 0 & 0 \\ 0 & -0.5 & 0 & -0.5 & 0 & 0 & 0 & 0 & 0 \\ 0 & 0 & -0.5 & 0 & 0 & 0 & -0.5 & 0 & 0 \\ 0 & 0 & 0 & 0 & -1 & 0 & 0 & 0 & 0 \\ 0 & 0 & 0 & 0 & 0 & -0.5 & 0 & -0.5 & 0 \\ 0 & 0 & 0 & 0 & 0 & 0 & 0 & 0 & -1 \end{pmatrix} \delta\begin{pmatrix} \partial a_1/\partial x_1 \\ \partial a_1/\partial x_2 \\ \partial a_1/\partial x_3 \\ \partial a_2/\partial x_1 \\ \partial a_2/\partial x_2 \\ \partial a_2/\partial x_3 \\ \partial a_3/\partial x_1 \\ \partial a_3/\partial x_2 \\ \partial a_3/\partial x_3 \end{pmatrix} \quad ; \tag{A-4}$$

and, the variance-covariance matrix of the gradient errors is, therefore, given by the diagonal matrix:

$$\boldsymbol{\Sigma}_{\Gamma} = \begin{pmatrix} -1 & 0 & 0 & 0 & 0 & 0 & 0 & 0 & 0 \\ 0 & -0.5 & 0 & -0.5 & 0 & 0 & 0 & 0 & 0 \\ 0 & 0 & -0.5 & 0 & 0 & 0 & -0.5 & 0 & 0 \\ 0 & 0 & 0 & 0 & -1 & 0 & 0 & 0 & 0 \\ 0 & 0 & 0 & 0 & 0 & -0.5 & 0 & -0.5 & 0 \\ 0 & 0 & 0 & 0 & 0 & 0 & 0 & 0 & -1 \end{pmatrix} \boldsymbol{\Sigma}_{\partial \boldsymbol{a}/\partial \boldsymbol{x}} \begin{pmatrix} -1 & 0 & 0 & 0 & 0 & 0 & 0 & 0 & 0 \\ 0 & -0.5 & 0 & -0.5 & 0 & 0 & 0 & 0 & 0 \\ 0 & 0 & -0.5 & 0 & 0 & 0 & -0.5 & 0 & 0 \\ 0 & 0 & 0 & 0 & -1 & 0 & 0 & 0 & 0 \\ 0 & 0 & 0 & 0 & 0 & -0.5 & 0 & -0.5 & 0 \\ 0 & 0 & 0 & 0 & 0 & 0 & 0 & 0 & -1 \end{pmatrix}^{\mathrm{T}} \tag{A-5}$$

$$= \begin{pmatrix} \sigma_{1,1}^2 & 0 & 0 & 0 & 0 & 0 \\ 0 & \frac{1}{4}\left(\sigma_{1,2}^2 + \sigma_{2,1}^2\right) & 0 & 0 & 0 & 0 \\ 0 & 0 & \frac{1}{4}\left(\sigma_{1,3}^2 + \sigma_{3,1}^2\right) & 0 & 0 & 0 \\ 0 & 0 & 0 & \sigma_{2,2}^2 & 0 & 0 \\ 0 & 0 & 0 & 0 & \frac{1}{4}\left(\sigma_{2,3}^2 + \sigma_{3,2}^2\right) & 0 \\ 0 & 0 & 0 & 0 & 0 & \sigma_{3,3}^2 \end{pmatrix}.$$

Appendix B

Covariance and psd models for the gravitational field are generally modeled using simple analytic functions that reflect certain desirable and required characteristics of the field. Either global (spherical) or local (planar) approximations are employed, depending on the application. Here we list only a planar (Cartesian) variation of the models, though corresponding spherical models can also be derived. Required characteristics include harmonic extension in altitude, stationarity of the field on any horizontal plane, and positive definiteness. Furthermore, the models of the auto- and cross-covariance functions among all quantities derived from the disturbing potential should be mutually self consistent. That is, we generally start with a certain model for the covariance function of the disturbing potential and all other models are derived from this according to the rules of propagation of covariances. If both spatial and spectral applications are contemplated, then it is also required that both the covariance and psd models in each case are Fourier transforms of each other. If one further desires to consider along-track psd's, then the psd in the two horizontal frequencies should be integrable (analytically) over each frequency.

All these properties are satisfied by the reciprocal distance covariance model that for the disturbing potential is given by

$$\phi_T\left(\Delta x_1,\Delta x_2; x_3,x_3'\right) = \frac{\sigma^2}{\sqrt{\left(1+\alpha\left(x_3+x_3'\right)\right)^2+\alpha^2 s^2}} \quad , \tag{B-1}$$

where σ, and α are parameters, and where

$$\Delta x_1 = x_1 - x_1' \, , \quad \Delta x_2 = x_2 - x_2' \quad , \tag{B-2}$$

and

$$s = \sqrt{\Delta x_1^2 + \Delta x_2^2} \quad . \tag{B-3}$$

Linear combinations of these types of models can be used to provide as much detail and refinement as necessary to characterize the stochastic correlation and spectrum of the field; see equation (64). We note that this covariance model is also isotropic since it depends only on the distance, *s*, between two points, not on the direction of one point with respect to the other. Isotropy is not a requirement but practically desirable. However, cross-covariances of derivatives are not necessarily isotropic, as will be seen below.

To simplify the notation, let us introduce the following:

$$\beta = 1 + \alpha\left(x_3 + x_3'\right) \, , \quad M = \beta^2 + \alpha^2 s^2 \quad , \tag{B-4}$$

and understand that all models are functions of $\left(\Delta x_1,\Delta x_2; x_3,x_3'\right)$, where the primed coordinates (see also equations (B-2)) always refer to the second function in the cross-covariance expression. Then

$$\phi_T = \frac{\sigma^2}{M^{1/2}} \ . \tag{B-5}$$

If f_j and g_k are two derivatives of T:

$$f_j = \frac{\partial T}{\partial x_j}, \quad g_k = \frac{\partial T}{\partial x_k'} \ , \tag{B-6}$$

then their covariance, according to the rules of propagation of covariances (Moritz, 1980), is given by

$$\phi_{f_j,g_k} = \frac{\partial^2 \phi_T}{\partial x_j \partial x_k'} \ . \tag{B-7}$$

Now, we introduce a further simplification in notation by letting $\partial T/\partial x_j \equiv T_{x_j}$ and $\partial^2 T/(\partial x_j \partial x_k) \equiv T_{x_j x_k}$. Then, for the first-order gradients of the disturbing potential,

$$\nabla T = \left(T_{x_1} \quad T_{x_2} \quad T_{x_3} \right)^{\mathrm{T}}, \tag{B-8}$$

we obtain the following auto-and cross-covariance models:

$$\phi_{T,T_{x_1}} = \frac{\sigma^2 \, \alpha^2 \, \Delta x_1}{M^{3/2}} = -\phi_{T_{x_1},T} \ ; \tag{B-9}$$

$$\phi_{T,T_{x_2}} = \frac{\sigma^2 \, \alpha^2 \, \Delta x_2}{M^{3/2}} = -\phi_{T_{x_2},T} \ ; \tag{B-10}$$

$$\phi_{T,\partial T/\partial x_3} = -\frac{\sigma^2 \, \alpha \, \beta}{M^{3/2}} = \phi_{\partial T/\partial x_3,T} \ ; \tag{B-11}$$

$$\phi_{\partial T/\partial x_1,\partial T/\partial x_1} = \frac{\sigma^2 \, \alpha^2}{M^{5/2}} \left(\beta^2 + \alpha^2 s^2 - 3\alpha^2 \Delta x_1^2 \right) \ ; \tag{B-12}$$

$$\phi_{\partial T/\partial x_1,\partial T/\partial x_2} = -3\,\frac{\sigma^2\,\alpha^4}{M^{5/2}}\Delta x_1\Delta x_2 = \phi_{\partial T/\partial x_2,\partial T/\partial x_1}\ ; \tag{B-13}$$

$$\phi_{\partial T/\partial x_1,\partial T/\partial x_3} = 3\,\frac{\sigma^2\,\alpha^3\,\beta}{M^{5/2}}\Delta x_1 = -\phi_{\partial T/\partial x_3,\partial T/\partial x_1}\ ; \tag{B-14}$$

$$\phi_{\partial T/\partial x_2,\partial T/\partial x_2} = \frac{\sigma^2\,\alpha^2}{M^{5/2}}\left(\beta^2 + \alpha^2 s^2 - 3\alpha^2\Delta x_2^2\right)\ ; \tag{B-15}$$

$$\phi_{\partial T/\partial x_2,\partial T/\partial x_3} = 3\,\frac{\sigma^2\,\alpha^3\,\beta}{M^{5/2}}\Delta x_2 = -\phi_{\partial T/\partial x_3,\partial T/\partial x_2}\ ; \tag{B-16}$$

$$\phi_{\partial T/\partial x_3,\partial T/\partial x_3} = \frac{\sigma^2\,\alpha^2}{M^{5/2}}\left(2\beta^2 - \alpha^2 s^2\right) = \phi_{\partial T/\partial x_1,\partial T/\partial x_1} + \phi_{\partial T/\partial x_2,\partial T/\partial x_2}\ . \tag{B-17}$$

For the second-order gradients, we note that since the gradient tensor is symmetric, any auto- or cross-covariance involving $\partial^2 T/(\partial x_j \partial x_k) \equiv T_{x_j x_k}$ is the same as the auto- or cross-covariance involving $\partial^2 T/(\partial x_k \partial x_j) \equiv T_{x_k x_j}$. We have:

$$\phi_{T,T_{x_1x_1}} = -\phi_{T_{x_1},T_{x_1}} = \phi_{T_{x_1x_1},T}\ ; \tag{B-18}$$

$$\phi_{T,T_{x_1x_2}} = -\phi_{T_{x_1},T_{x_2}} = \phi_{T_{x_1x_2},T}\ ; \tag{B-19}$$

$$\phi_{T,T_{x_1x_3}} = -\phi_{T_{x_1},T_{x_3}} = -\phi_{T_{x_1x_3},T}\ ; \tag{B-20}$$

$$\phi_{T,T_{x_2x_2}} = -\phi_{T_{x_2},T_{x_2}} = \phi_{T_{x_2x_2},T}\ ; \tag{B-21}$$

$$\phi_{T,T_{x_2x_3}} = -\phi_{T_{x_2},T_{x_3}} = -\phi_{T_{x_2x_3},T}\ ; \tag{B-22}$$

$$\phi_{T,T_{x_3x_3}} = \phi_{T_{x_3},T_{x_3}} = \phi_{T_{x_3x_3},T}\ ; \tag{B-23}$$

$$\phi_{T_{x_1},T_{x_1x_1}} = \frac{3\sigma^2\,\alpha^4\Delta x_1}{M^{7/2}}\left(3\beta^2 + 3\alpha^2 s^2 - 5\alpha^2\Delta x_1^2\right) = -\phi_{T_{x_1x_1},T_{x_1}}\ ; \tag{B-24}$$

$$\phi_{T_{x_1},T_{x_1x_2}} = \frac{3\sigma^2\,\alpha^4\Delta x_2}{M^{7/2}}\left(\beta^2 + \alpha^2 s^2 - 5\alpha^2\Delta x_1^2\right) = -\,\phi_{T_{x_1x_2},T_{x_1}} = \phi_{T_{x_2},T_{x_1x_1}} = -\,\phi_{T_{x_1x_1},T_{x_2}}\ ; \qquad \text{(B-25)}$$

$$\phi_{T_{x_1},T_{x_1x_3}} = \frac{3\sigma^2\,\alpha^3\,\beta}{M^{7/2}}\left(-\beta^2 - \alpha^2 s^2 + 5\alpha^2\Delta x_1^2\right) = \phi_{T_{x_1x_3},T_{x_1}} = -\,\phi_{T_{x_3},T_{x_1x_1}} = -\,\phi_{T_{x_1x_1},T_{x_3}}\ ; \qquad \text{(B-26)}$$

$$\phi_{T_{x_1},T_{x_2x_2}} = \frac{3\sigma^2\,\alpha^4\Delta x_2}{M^{7/2}}\left(\beta^2 + \alpha^2 s^2 - 5\alpha^2\Delta x_2^2\right) = -\,\phi_{T_{x_2x_2},T_{x_1}} = \phi_{T_{x_2},T_{x_1x_2}} = -\,\phi_{T_{x_1x_2},T_{x_2}}\ ; \qquad \text{(B-27)}$$

$$\phi_{T_{x_1},T_{x_2x_3}} = \frac{15\sigma^2\,\alpha^5\,\beta}{M^{7/2}}\Delta x_1\Delta x_2 = \phi_{T_{x_2x_3},T_{x_1}} = -\,\phi_{T_{x_3},T_{x_1x_2}} = \phi_{T_{x_2},T_{x_1x_3}} = -\,\phi_{T_{x_1x_2},T_{x_3}} = \phi_{T_{x_1x_3},T_{x_2}}\ ; \qquad \text{(B-28)}$$

$$\phi_{T_{x_1},T_{x_3x_3}} = \frac{3\sigma^2\,\alpha^4\Delta x_1}{M^{7/2}}\left(-4\beta^2 + \alpha^2 s^2\right) = -\,\phi_{T_{x_3x_3},T_{x_1}} = -\,\phi_{T_{x_3},T_{x_1x_3}} = \phi_{T_{x_1x_3},T_{x_3}}\ ; \qquad \text{(B-29)}$$

$$\phi_{T_{x_2},T_{x_2x_2}} = \frac{3\sigma^2\,\alpha^4\Delta x_2}{M^{7/2}}\left(3\beta^2 + 3\alpha^2 s^2 - 5\alpha^2\Delta x_2^2\right) = -\,\phi_{T_{x_2x_2},T_{x_2}}\ ; \qquad \text{(B-30)}$$

$$\phi_{T_{x_2},T_{x_2x_3}} = \frac{3\sigma^2\,\alpha^3\,\beta}{M^{7/2}}\left(-\beta^2 - \alpha^2 s^2 + 5\alpha^2\Delta x_2^2\right) = \phi_{T_{x_2x_3},T_{x_2}} = -\,\phi_{T_{x_3},T_{x_2x_2}} = -\,\phi_{T_{x_2x_2},T_{x_3}}\ ; \qquad \text{(B-31)}$$

$$\phi_{T_{x_2},T_{x_3x_3}} = \frac{3\sigma^2\,\alpha^4\Delta x_2}{M^{7/2}}\left(-4\beta^2 + \alpha^2 s^2\right) = -\,\phi_{T_{x_3x_3},T_{x_2}} = -\,\phi_{T_{x_3},T_{x_2x_3}} = \phi_{T_{x_2x_3},T_{x_3}}\ ; \qquad \text{(B-32)}$$

$$\phi_{T_{x_3},T_{x_3x_3}} = \frac{3\sigma^2\,\alpha^3\,\beta}{M^{7/2}}\left(-2\beta^2 + 3\alpha^2 s^2\right) = \phi_{T_{x_3x_3},T_{x_3}}\ ; \qquad \text{(B-33)}$$

$$\phi_{T_{x_1x_1},T_{x_1x_1}} = \frac{3\sigma^2\,\alpha^4}{M^{9/2}}\left(3M^2 - 30M\alpha^2\Delta x_1^2 + 35\alpha^4\Delta x_1^4\right)\ ; \qquad \text{(B-34)}$$

$$\phi_{T_{x_1x_1},T_{x_1x_2}} = \frac{15\sigma^2\,\alpha^6\,\Delta x_1\Delta x_2}{M^{9/2}}\left(-3M + 7\alpha^2\Delta x_1^2\right) = \phi_{T_{x_1x_2},T_{x_1x_1}}\ ; \qquad \text{(B-35)}$$

$$\phi_{T_{x_1x_1},T_{x_1x_3}} = \frac{15\sigma^2\,\alpha^5\,\beta\,\Delta x_1}{M^{9/2}}\left(3M - 7\alpha^2\Delta x_1^2\right) = -\,\phi_{T_{x_1x_3},T_{x_1x_1}}\ ; \tag{B-36}$$

$$\phi_{T_{x_1x_1},T_{x_2x_2}} = \frac{3\sigma^2\,\alpha^4}{M^{9/2}}\left(M^2 - 5\alpha^2 s^2 M + 35\alpha^4\Delta x_1^2\Delta x_2^2\right) = \phi_{T_{x_2x_2},T_{x_1x_1}} = \phi_{T_{x_1x_2},T_{x_1x_2}}\ ; \tag{B-37}$$

$$\phi_{T_{x_1x_1},T_{x_2x_3}} = \frac{15\sigma^2\,\alpha^5\,\beta\,\Delta x_2}{M^{9/2}}\left(M - 7\alpha^2\Delta x_1^2\right) = -\,\phi_{T_{x_2x_3},T_{x_1x_1}} = -\,\phi_{T_{x_1x_3},T_{x_1x_2}} = \phi_{T_{x_1x_2},T_{x_1x_3}}\ ; \tag{B-38}$$

$$\phi_{T_{x_1x_1},T_{x_3x_3}} = \frac{3\sigma^2\,\alpha^4}{M^{9/2}}\left(-4M^2 + 5M\alpha^2\Delta x_2^2 + 35\beta^2\alpha^2\Delta x_1^2\right) = \phi_{T_{x_3x_3},T_{x_1x_1}} = -\,\phi_{T_{x_1x_3},T_{x_1x_3}}\ ; \tag{B-39}$$

$$\phi_{T_{x_1x_2},T_{x_2x_2}} = \frac{15\sigma^2\,\alpha^6\,\Delta x_1\Delta x_2}{M^{9/2}}\left(-3M + 7\alpha^2\Delta x_2^2\right) = \phi_{T_{x_2x_2},T_{x_1x_2}}\ ; \tag{B-40}$$

$$\phi_{T_{x_1x_2},T_{x_2x_3}} = \frac{15\sigma^2\,\alpha^5\,\beta\,\Delta x_1}{M^{9/2}}\left(M - 7\alpha^2\Delta x_2^2\right) = -\,\phi_{T_{x_2x_3},T_{x_1x_2}} = -\,\phi_{T_{x_1x_3},T_{x_2x_2}} = \phi_{T_{x_2x_2},T_{x_1x_3}}\ ; \tag{B-41}$$

$$\phi_{T_{x_1x_2},T_{x_3x_3}} = \frac{15\sigma^2\,\alpha^6\,\Delta x_1\Delta x_2}{M^{9/2}}\left(-M + 7\beta^2\right) = \phi_{T_{x_3x_3},T_{x_1x_2}} = -\,\phi_{T_{x_1x_3},T_{x_2x_3}} = -\,\phi_{T_{x_2x_3},T_{x_1x_3}}\ ; \tag{B-42}$$

$$\phi_{T_{x_1x_3},T_{x_3x_3}} = \frac{15\sigma^2\,\alpha^5\,\beta\,\Delta x_1}{M^{9/2}}\left(-3M + 7\beta^2\right) = -\,\phi_{T_{x_3x_3},T_{x_1x_3}}\ ; \tag{B-43}$$

$$\phi_{T_{x_2x_2},T_{x_2x_2}} = \frac{3\sigma^2\,\alpha^4}{M^{9/2}}\left(3M^2 - 30M\alpha^2\Delta x_2^2 + 35\alpha^4\Delta x_2^4\right)\ ; \tag{B-44}$$

$$\phi_{T_{x_2x_2},T_{x_2x_3}} = \frac{15\sigma^2\,\alpha^5\,\beta\,\Delta x_2}{M^{9/2}}\left(3M - 7\alpha^2\Delta x_2^2\right) = -\,\phi_{T_{x_2x_3},T_{x_2x_2}}\ ; \tag{B-45}$$

$$\phi_{T_{x_2x_2},T_{x_3x_3}} = \frac{3\sigma^2\,\alpha^4}{M^{9/2}}\left(-4M^2 + 5M\alpha^2\Delta x_1^2 + 35\beta^2\alpha^2\Delta x_2^2\right) = \phi_{T_{x_3x_3},T_{x_2x_2}} = -\,\phi_{T_{x_2x_3},T_{x_2x_3}}\ ; \tag{B-46}$$

$$\phi_{T_{x_2x_3},T_{x_3x_3}} = \frac{15\sigma^2\,\alpha^5\,\beta\,\Delta x_2}{M^{9/2}}\left(-3M+7\beta^2\right) = -\,\phi_{T_{x_3x_3},T_{x_2x_3}}\ ; \tag{B-47}$$

$$\phi_{T_{x_3x_3},T_{x_3x_3}} = \frac{3\sigma^2\,\alpha^4}{M^{9/2}}\left(8\beta^2-24\beta^2\alpha^2s^2+3\alpha^4s^4\right) = \phi_{T_{x_1x_3},T_{x_1x_3}} + \phi_{T_{x_2x_3},T_{x_2x_3}}\ . \tag{B-48}$$

The power spectral densities (psd's) corresponding to these covariance models are easily determined from the basic psd of the disturbing potential, the Fourier transform of equation (B-5):

$$\Phi_T\left(\mu_1,\mu_2;\,x_3,x_3'\right) = \frac{\sigma^2}{\alpha\,\mu}\,\mathrm{e}^{-2\pi\mu\alpha^{-1}}\,\mathrm{e}^{-2\pi\mu\left(x_3+x_3'\right)}\ , \tag{B-49}$$

where the magnitude of spatial frequencies, μ_1 and μ_2, is given by

$$\mu = \sqrt{\mu_1^2+\mu_2^2}\ . \tag{B-50}$$

That Φ_T depends only on μ is a consequence of ϕ_T depending only on s (isotropy). The inverse Fourier transform of Φ_T is ϕ_T:

$$\phi_T\left(\Delta x_1,\Delta x_2;\,x_3,x_3'\right) = \int_{-\infty}^{\infty}\!\!\int \frac{\sigma^2}{\alpha\,\mu}\,\mathrm{e}^{-2\pi\mu\alpha^{-1}}\,\mathrm{e}^{-2\pi\mu\left(x_3+x_3'\right)}\,\mathrm{e}^{i2\pi\left(\mu_1\Delta x_1+\mu_2\Delta x_2\right)}\,d\mu_1\,d\mu_2\ . \tag{B-51}$$

In fact, the covariance between any two quantities is related to the psd of the same quantities by a transform like equation (B-51). Thus, applying the propagation of covariances, equation (B-7), we find that for each derivative with respect to x_j, $j=1,2$, we multiply Φ_T by $i2\pi\mu_j$, and for each derivative with respect to x_k', $k=1,2$, we multiply Φ_T by $-i2\pi\mu_k$. For derivatives with respect to x_3 or x_3', we multiply Φ_T by $-2\pi\mu$. It can be proved (Jekeli, 2001) that these rules hold in general, not just for this particular model.

Consider the covariance of the q^{th} derivative of T with respect to variable, x_j and the r^{th} derivative of T with respect to the variable, x_k'. Again, omitting the arguments, $\left(\mu_1,\mu_2;\,x_3,x_3'\right)$, we have the following general result for the corresponding psd:

$$\mathrm{psd}\left(\partial^qT/\left((\partial x_{j_1})^{q_1}(\partial x_{j_2})^{q_2}\right),\partial^rT/\left((\partial x_{k_1}')^{r_1}(\partial x_{k_2}')^{r_2}\right)\right) = (\lambda_{j_1})^{q_1}\,(\lambda_{j_2})^{q_2}\,(\lambda_{k_1}^*)^{r_1}\,(\lambda_{k_2}^*)^{r_2}\,\Phi_T\ ; \tag{B-52}$$

where * denotes complex conjugate, the indices satisfy

$$j_1, j_2, k_1, k_2 \in \{1,2,3\}\ ; \quad q, q_1, q_2, r, r_1, r_2 \in \{0,1,2\}\ , \quad q = q_1 + q_2\ , \quad r = r_1 + r_2\ ; \quad \text{(B-53)}$$

and where

$$\lambda_m = i2\pi\mu_m\ , \quad \text{if} \quad m = 1,2\ ; \quad \text{and} \quad \lambda_3 = -2\pi\mu\ . \quad \text{(B-54)}$$

Appendix C

The hybrid psd/covariance function of the disturbing potential on a plane is defined as the psd with respect to the first variable and the covariance with respect to the second variable. That is, we take the 2-D psd and apply the inverse Fourier transform with respect to the second variable, or equivalently, we take the Fourier transform of the covariance with respect to the first variable:

$$S_T\left(\mu_1;\, \Delta x_2;\, x_3,x_3'\right) = \int_{-\infty}^{\infty} \Phi_T\left(\mu_1,\, \mu_2;\, x_3,x_3'\right) \mathrm{e}^{\,i\,2\pi\mu_2\Delta x_2} d\mu_2$$

$$= \int_{-\infty}^{\infty} \phi_T\left(\Delta x_1,\, \Delta x_2;\, x_3,x_3'\right) \mathrm{e}^{-i\,2\pi\mu_1\Delta x_1}\, d\Delta x_1\,, \tag{C-1}$$

The reciprocal distance model, equations (B-5), (B-49), can be integrated to yield these hybrid functions in analytic form. Most of these were given by Stanley K.Jordan (1982, unpublished manuscript). For the disturbing potential, *T*, we have:

$$S_T\left(\mu_1;\, \Delta x_2;\, x_3,x_3'\right) = \frac{2\,\sigma^2}{\alpha}\, K_0\left(2\pi\mu_1 d\right)\ , \tag{C-2}$$

where K_0 is the modified Bessel function of the second kind and zero order, and

$$d = \sqrt{\frac{\beta^2}{\alpha^2} + \Delta x_2^2}\ . \tag{C-3}$$

For the various derivatives of the disturbing potential, it can be shown that the corresponding hybrid psd/covariance models have the following forms. Again, the arguments, $\left(\mu_1;\, \Delta x_2;\, x_3,x_3'\right)$, are omitted for simplicity in notation:

$$S_{T,T_{x_1}} = i2\pi\mu_1\, S_T = -\,S_{T_{x_1},T}\ ; \tag{C-4}$$

$$S_{T,T_{x_2}} = -\,\frac{2\sigma^2\left(2\pi\mu_1\right)\Delta x_2}{\alpha\, d}\, K_1\left(2\pi\mu_1 d\right) = -\,S_{T_{x_2},T}\ , \tag{C-5}$$

where K_1 is the modified Bessel function of the second kind and first order;

$$S_{T,T_{x_3}} = -\frac{2\sigma^2\left(2\pi\mu_1\right)\beta}{\alpha^2 d} K_1\left(2\pi\mu_1 d\right) = S_{T_{x_3},T} \ ; \tag{C-6}$$

$$S_{T_{x_1},T_{x_1}} = \left(2\pi\mu_1\right)^2 S_T \ ; \tag{C-7}$$

$$S_{T_{x_1},T_{x_2}} = i2\pi\mu_1 S_{T_{x_2},T} = S_{T_{x_2},T_{x_1}} \ ; \tag{C-8}$$

$$S_{T_{x_1},T_{x_3}} = -i2\pi\mu_1 S_{T,T_{x_3}} = -S_{T_{x_3},T_{x_1}} \ ; \tag{C-9}$$

$$S_{T_{x_2},T_{x_2}} = \frac{2\sigma^2\left(2\pi\mu_1\right)}{\alpha d}\left(\left(1-\frac{2\Delta x_2^2}{d^2}\right)K_1\left(2\pi\mu_1 d\right) - 2\pi\mu_1\frac{\Delta x_2^2}{d} K_0\left(2\pi\mu_1 d\right)\right) \ ; \tag{C-10}$$

$$S_{T_{x_2},T_{x_3}} = -\frac{2\sigma^2\left(2\pi\mu_1\right)\beta\,\Delta x_2}{\alpha^2 d^3}\left(2\,K_1\left(2\pi\mu_1 d\right) + 2\pi\mu_1\, d\, K_0\left(2\pi\mu_1 d\right)\right) = -S_{T_{x_3},T_{x_2}} \ ; \tag{C-11}$$

$$S_{T_{x_3},T_{x_3}} = S_{T_{x_1},T_{x_1}} + S_{T_{x_2},T_{x_2}} \ . \tag{C-12}$$

$$S_{T,T_{x_1x_1}} = -S_{T_{x_1},T_{x_1}} = S_{T_{x_1x_1},T} \ ; \tag{C-13}$$

$$S_{T,T_{x_1x_2}} = -S_{T_{x_1},T_{x_2}} = S_{T_{x_1x_2},T} \ ; \tag{C-14}$$

$$S_{T,T_{x_1x_3}} = -S_{T_{x_1},T_{x_3}} = -S_{T_{x_1x_3},T} \ ; \tag{C-15}$$

$$S_{T,T_{x_2x_2}} = -S_{T_{x_2},T_{x_2}} = S_{T_{x_2x_2},T} \ ; \tag{C-16}$$

$$S_{T,T_{x_2x_3}} = -S_{T_{x_2},T_{x_3}} = -S_{T_{x_2x_3},T} \ ; \tag{C-17}$$

$$S_{T,T_{x_3x_3}} = S_{T_{x_3},T_{x_3}} = S_{T_{x_3x_3},T} \ ; \tag{C-18}$$

$$S_{T_{x_1},T_{x_1x_1}} = i\left(2\pi\mu_1\right)^3 S_T = -S_{T_{x_1x_1},T_{x_1}} \ ; \tag{C-19}$$

$$S_{T_{x_1},T_{x_1x_2}} = \left(2\pi\mu_1\right)^2 S_{T,T_{x_2}} = -S_{T_{x_1x_2},T_{x_1}} = S_{T_{x_2},T_{x_1x_1}} = -S_{T_{x_1x_1},T_{x_2}} \ ; \tag{C-20}$$

$$S_{T_{x_1},\partial^2 T/(\partial x_1 \partial x_3)} = \left(2\pi\mu_1\right)^2 S_{T,T_{x_3}} = S_{T_{x_1x_3},T_{x_1}} = -S_{T_{x_3},T_{x_1x_1}} = -S_{T_{x_1x_1},T_{x_3}} \ ; \tag{C-21}$$

$$S_{T_{x_1},T_{x_2x_2}} = i2\pi\mu_1 S_{T_{x_2},T_{x_2}} = -S_{T_{x_2x_2},T_{x_1}} = S_{T_{x_2},T_{x_1x_2}} = -S_{T_{x_1x_2},T_{x_2}} \ ; \tag{C-22}$$

$$S_{T_{x_1},T_{x_2x_3}} = i2\pi\mu_1 S_{T_{x_2},T_{x_3}} = S_{T_{x_2x_3},T_{x_1}} = -S_{T_{x_3},T_{x_1x_2}} = S_{T_{x_2},T_{x_1x_3}} = -S_{T_{x_1x_2},T_{x_3}} = S_{T_{x_1x_3},T_{x_2}} \ ; \tag{C-23}$$

$$S_{T_{x_1},T_{x_3x_3}} = -i2\pi\mu_1 S_{T_{x_3},T_{x_3}} = -S_{T_{x_3x_3},T_{x_1}} = -S_{T_{x_3},T_{x_1x_3}} = S_{T_{x_1x_3},T_{x_3}} \ ; \tag{C-24}$$

$$\begin{aligned} S_{T_{x_2},T_{x_2x_2}} &= -\frac{2\sigma^2\left(2\pi\mu_1\right)\Delta x_2}{\alpha\, d^3} \\ &\left(\left(6-\frac{8\Delta x_2^2}{d^2}-\left(2\pi\mu_1\Delta x_2\right)^2\right)K_1\left(2\pi\mu_1 d\right)+2\pi\mu_1 d\left(3-\frac{4\Delta x_2^2}{d^2}\right)K_0\left(2\pi\mu_1 d\right)\right) \\ &= -S_{T_{x_2x_2},T_{x_2}} \end{aligned} \ ; \tag{C-25}$$

$$\begin{aligned} S_{T_{x_2},T_{x_2x_3}} &= -\frac{2\sigma^2\left(2\pi\mu_1\right)\beta}{\alpha^2\, d^3} \\ &\left(\left(2-\frac{8\Delta x_2^2}{d^2}-\left(2\pi\mu_1\Delta x_2\right)^2\right)K_1\left(2\pi\mu_1 d\right)+2\pi\mu_1 d\left(1-\frac{4\Delta x_2^2}{d^2}\right)K_0\left(2\pi\mu_1 d\right)\right) \\ &= S_{T_{x_2x_3},T_{x_2}} = -S_{\partial T/\partial x_3,T_{x_2x_2}} = -S_{T_{x_2x_2},\partial T/\partial x_3} \ ; \end{aligned} \tag{C-26}$$

$$S_{T_{x_2},T_{x_3x_3}} = -S_{T_{x_2},T_{x_1x_1}} - S_{T_{x_2},T_{x_2x_2}} = -S_{T_{x_3x_3},T_{x_2}} = -S_{T_{x_3},T_{x_2x_3}} = S_{T_{x_2x_3},T_{x_3}} \ ; \tag{C-27}$$

$$S_{T_{x_3},T_{x_3x_3}} = S_{T_{x_1},T_{x_1x_3}} + S_{T_{x_2},T_{x_2x_3}} = S_{T_{x_3x_3},T_{x_3}} \ ; \tag{C-28}$$

$$S_{T_{x_1x_1},T_{x_1x_1}} = \left(2\pi\mu_1\right)^4 S_T \ ; \tag{C-29}$$

$$\phi_{T_{x_1x_1},T_{x_1x_2}} = i\left(2\pi\mu_1\right)^3 S_{T_{x_2},T} = S_{T_{x_1x_2},T_{x_1x_1}} \ ; \tag{C-30}$$

$$S_{T_{x_1x_1},T_{x_1x_3}} = -i\left(2\pi\mu_1\right)^3 S_{T,T_{x_3}} = -S_{T_{x_1x_3},T_{x_1x_1}} \ ; \tag{C-31}$$

$$\phi_{T_{x_1x_1},T_{x_2x_2}} = \left(2\pi\mu_1\right)^2 S_{T_{x_2},T_{x_2}} = S_{T_{x_2x_2},T_{x_1x_1}} = S_{T_{x_1x_2},T_{x_1x_2}} \ ; \tag{C-32}$$

$$S_{T_{x_1x_1},T_{x_2x_3}} = \left(2\pi\mu_1\right)^2 S_{T_{x_2},T_{x_3}} = -S_{T_{x_2x_3},T_{x_1x_1}} = -S_{T_{x_1x_3},T_{x_1x_2}} = S_{T_{x_1x_2},T_{x_1x_3}} \ ; \tag{C-33}$$

$$S_{T_{x_1x_1},T_{x_3x_3}} = -\left(2\pi\mu_1\right)^2 S_{T_{x_3},T_{x_3}} = S_{T_{x_3x_3},T_{x_1x_1}} = -S_{T_{x_1x_3},T_{x_1x_3}} \ ; \tag{C-34}$$

$$S_{T_{x_1x_2},T_{x_2x_2}} = i2\pi\mu_1 S_{T_{x_2x_2},T_{x_2}} = S_{T_{x_2x_2},T_{x_1x_2}} \ ; \tag{C-35}$$

$$S_{T_{x_1x_2},T_{x_2x_3}} = -i2\pi\mu_1 S_{T_{x_2},T_{x_2x_3}} = -S_{T_{x_2x_3},T_{x_1x_2}} = -S_{T_{x_1x_3},T_{x_2x_2}} = S_{T_{x_2x_2},T_{x_1x_3}} \ ; \tag{C-36}$$

$$S_{T_{x_1x_2},T_{x_3x_3}} = -i2\pi\mu_1 S_{T_{x_2x_3},T_{x_3}} = S_{T_{x_3x_3},T_{x_1x_2}} = -S_{T_{x_1x_3},T_{x_2x_3}} = -S_{T_{x_2x_3},T_{x_1x_3}} \ ; \tag{C-37}$$

$$S_{T_{x_1x_3},T_{x_3x_3}} = S_{T_{x_1x_1},T_{x_1x_3}} - S_{T_{x_1x_3},T_{x_2x_2}} = -S_{T_{x_3x_3},T_{x_1x_3}} \ ; \tag{C-38}$$

$$\begin{aligned} S_{T_{x_2x_2},T_{x_2x_2}} = \frac{2\sigma^2\left(2\pi\mu_1\right)}{\alpha d^3}\Bigg(& 2\pi\mu_1 d\left(3 - \frac{24\Delta x_2^2}{d^2} + \frac{24\Delta x_2^4}{d^4} + \left(2\pi\mu_1\Delta x_2\right)^2\frac{\Delta x_2^2}{d^2}\right)K_0\left(2\pi\mu_1 d\right) \\ & + 2\left(3 - \frac{24\Delta x_2^2}{d^2} - 3\left(2\pi\mu_1\Delta x_2\right)^2 + \frac{24\Delta x_2^4}{d^4} + 4\left(2\pi\mu_1\Delta x_2\right)^2\frac{\Delta x_2^2}{d^2}\right)K_1\left(2\pi\mu_1 d\right)\Bigg); \end{aligned} \tag{C-39}$$

$$S_{T_{x_2x_2},T_{x_2x_3}} = -\frac{2\sigma^2\left(2\pi\mu_1\right)\beta\,\Delta x_2}{\alpha^2\,d^5}\left(2\pi\mu_1 d\left(12-\frac{24\Delta x_2^2}{d^2}-\left(2\pi\mu_1\Delta x_2\right)^2\right)K_0\left(2\pi\mu_1 d\right)\right.$$

$$\left.+\left(24-\frac{48\Delta x_2^2}{d^2}+3\left(2\pi\mu_1 d\right)^2-8\left(2\pi\mu_1\Delta x_2\right)^2\right)K_1\left(2\pi\mu_1 d\right)\right) \qquad \text{(C-40)}$$

$$= -S_{T_{x_2x_3},T_{x_2x_2}};$$

$$S_{T_{x_2x_2},T_{x_3x_3}} = -S_{T_{x_1x_1},T_{x_2x_2}} - S_{T_{x_2x_2},T_{x_2x_2}} = S_{T_{x_3x_3},T_{x_2x_2}} = -S_{T_{x_2x_3},T_{x_2x_3}}\ ; \qquad \text{(C-41)}$$

$$S_{T_{x_2x_3},T_{x_3x_3}} = S_{T_{x_1x_1},T_{x_2x_3}} + S_{T_{x_2x_2},T_{x_2x_3}} = -S_{T_{x_3x_3},T_{x_2x_3}}\ ; \qquad \text{(C-42)}$$

$$S_{T_{x_3x_3},T_{x_3x_3}} = S_{T_{x_1x_3},T_{x_1x_3}} + S_{T_{x_2x_3},T_{x_2x_3}}\ . \qquad \text{(C-43)}$$

References

Abramowitz, M. and I.A. Stegun (1972): *Handbook of Mathematical Functions*. Dover Publ., Inc., New York.

Bona, P. (2000): Precision, cross correlation and time correlation of GPS phase and code observations. *GPS Solutions*, **4**(2), 3-13.

Bona, P. and Tiberius, C. (2000): An experimental comparison of noise characteristics of seven high-end dual frequency GPS receiver sets. Proc. IEEE PLANS2000, 13-16 March 2000, San Diego, California, pp.237-244.

Grejner-Brzezinska, D., R. Da, and C.Toth (1998): GPS error modeling and OTF ambiguity resolution for high-accuracy GPS/INS integrated system. *Journal of Geodesy*, **72**(11), 626-638.

Heiskanen W.A. and H. Moritz (1976): *Physical Geodesy*. W.H. Freeman, San Francisco.

Jekeli, C. (1984): Analysis of airborne Gravity Gradiometer Survey System accuracy. *Manuscripta Geodaetica*, **9**(4), 323-379.

Jekeli, C. (1988): The Gravity Gradiometer Survey System. *EOS, Trans. Am. Geophys. Union*, **69** (8), 105, 116-117.

Jekeli, C. (1992): Vector Gravimetry Using GPS in Free-Fall and in an Earth-Fixed Frame. *Bulletin Geodesique*, **66**(1), 54-61.

Jekeli, C. (1995): Airborne Vector Gravimetry Using Precise, Position-Aided Inertial Measurement Units. *Bulletin Géodésique*, **69**(1), 1-11.

Jekeli, C. (2000): *Inertial Navigation Systems with Geodetic Applications.* W. DeGruyter, Berlin.

Jekeli, C. (2001): *Fourier Geodesy*. Lecture notes, Laboratory for Space Geodesy and Remote Sensing Research, Geodetic Science, Ohio State University, Columbus, Ohio.

Jekeli, C. and J.H. Kwon (2001): Analysis and Processing of Svalbard Airborne INS/GPS Data for Vector Gravimetry. Interim technical report, NIMA contract NMA202-98-1-1110, OSU Project 736145.

Lemoine, F.G. et al. (1998): The development of the joint NASA GSFC and the National Imagery Mapping Agency (NIMA) geopotential model EGM96. NASA Technical Report NASA/TP-1998- 206861, Goddard Space Flight Center, Greenbelt, Maryland.

Moritz, H. (1980): *Advanced Physical Geodesy*. Abacus press, Tunbridge Wells, Kent.

Nettleton, L.L. (1976): *Gravity and Magnetics in Oil Prospecting*. McGraw Hill, Inc., New York.

Paik, H.J., E.R. Canavan, and M.V. Moody (1997): Airborne/shipborne SGG survey system. Proceedings of the International Symposium on Kinematic Systems in Geodesy, Geomatics, and Navigation, 3-6 June 1997, Banff, Canada, pp.565-570.

Papoulis, A. (1977): *Signal Analysis*, McGraw Hill, New York.

Priestley, M.B. (1981): *Spectral Analysis and Time Series Analysis*, Academic Press, New York.

Schwarz, K.P., O.L. Colombo, G. Hein, and E.T. Kmickmeyer (1992): Requirements for airborne vector gravimetry. Proc. IAG Symp., From Mars to Greenland: Charting Gravity

with Space and Airborne Instruments, General Assembly of the IUGG, Vienna, 1991, Springer Verlag, New York, pp.273-283.

Talwani, M.: http://www.geophysics.rice.edu/department/faculty/talwani/sanandreas.html.

Zorn, A.H. (2002): A merging of system technologies – all-accelerometer inertial navigation and gravity gradiometry. Presented at IEEE Position Location and Navigation Symposium (PLANS) 2002, Palm Springs, California, 15-18 April 2002.